AFCRL-71-0067

Seasonal Variations of the Inter-Tropical Convergence Zone
Studied with an Interacting Atmosphere and Ocean Model

by

Arthur C. Pike

Rosenstiel School of Marine and Atmospheric Science
Division of Atmospheric Science
University of Miami
Coral Gables, Florida 33124

DDC

AD720266

49

# DISCLAIMER NOTICE

DEFENSE TECHNICAL INFORMATION CENTER

THIS DOCUMENT IS BEST QUALITY AVAILABLE. THE COPY FURNISHED TO DTIC CONTAINED A SIGNIFICANT NUMBER OF PAGES WHICH DO NOT REPRODUCE LEGIBLY.

Qualified requestors may obtain additional copies from the Defense
Documentation Center. All others should apply to the National Technical
Information Service.

Seasonal Variations of the Inter-Tropical Convergence Zone
Studied with an Interacting Atmosphere and Ocean Model

by

Arthur C. Pike

Rosenstiel School of Marine and Atmospheric Science
Division of Atmospheric Science
University of Miami
Coral Gables, Florida   33124

Abstract


        A simple, four-level primitive-equation model of a zonally-
symmetric tropical atmosphere has been combined with a two-layer
model of the upper tropical ocean in order to predict three years of
inter-tropical convergence zone (ITCZ) behavior under the influence
of seasonally-variable solar heating of the sea. A cold equatorial
surface develops on account of oceanic upwelling and vertical mixing;
a single ITCZ establishes itself, off the equator, over the surface
temperature maximum in the warmer hemisphere. This convergence zone
migrates quickly between hemispheres, with only a minor lag, when the
progress of the seasons causes the hemispheric surface temperature
asymmetry to reverse every half year. Such behavior is qualitatively
in accord with that of the updraft branch of the mean tropical Hadley
circulation in the real atmosphere. The lag of maximum sub-equatorial
sea surface temperature behind the overhead sun of late summer is com-
puted to be about nine weeks, a reasonable value.

## Table of Contents

## List of Figures

## 1. Introduction

This paper is a continuation of studies by Pike (1968, 1970) involving numerical modelling of the atmospheric inter-tropical convergence zone (ITCZ) with the primitive equations. It was found in the earlier study that, at least over the sea, the maximum upward motion and precipitation rate associated with the ITCZ occurred at or very near the latitude of maximum surface temperature. In particular, a notable equatorial depression of surface temperature compared to that at a higher latitude seemed to be essential if the ITCZ were to reach an equilibrium location away from the equator. These early numerical experiments were conducted with a ten-level, zonally-symmetric atmospheric model with prescribed latitudinal surface temperature profiles. In contrast, Bates (1970) obtained stable moist ITCZ's off the equator with no such depression; but an assumption of no available equatorial moisture [his eq. 24] excluded a moist ITCZ there a priori. Bates's dry ITCZ did form on the equator.

It was then realized that the surface temperature distribution, especially at sea, is not at all independent of atmospheric factors; the pattern of wind stress on the sea surface will strongly influence the upper ocean current system and its associated horizontal divergence. The resulting field of oceanic vertical motion, in conjunction with the well-known decrease of temperature with depth in the sea, can produce anomalously cold surface temperatures by means of upwelling. The development of relatively vigorous wind-driven ocean currents in themselves can, of course, induce substantial vertical turbulent mixing which would tend to lower the surface temperature. In a reverse sense, the direct thermodynamic effect of the surface temperature pattern on the atmosphere is sure to affect its hydrostatic pressure gradient and the associated wind and wind stress fields; there is a continuous two-way interaction between air and sea. It seemed desirable, therefore, to have the surface temperature a predicted rather than fixed quantity in any model whose behavior is strongly dependent on it. At sea, prediction of surface temperature requires approximation of the circulation of the upper ocean; a simple, highly-parameterized two-layer ocean model substantially the same as that described in section 4 was developed for this purpose. It was combined with the ten-level air model to make a fully-interacting two-fluid numerical experiment over 88 days; the surface temperature profile, initially flat, showed the progressive development of a cold equator on account of upwelling and vertical mixing of cold water. A single ITCZ established itself at first over the equator but then migrated poleward as the equator cooled; the convergence zone remained single, showing great stability, despite the eventual double surface temperature maximum.

A numerical integration of this kind of two-fluid model over a period of several years seemed desirable in order to investigate the degree of stability of the single off-equatorial ITCZ under the influence of seasonally variable solar heating of the sea. As about 30 hours of CDC 6600 computer time would have been required for a one year prediction with the two-fluid model as it then was constituted, simplification was indicated for purposes of economy. Since the oceanic part was really as basic as could be safely attempted in temperature prediction involving dynamic factors, only the atmospheric part was a suitable

candidate for reduction in complexity. The stripped-down air model discussed in section 3 has only four atmospheric levels and handles frictional and convective processes in a much simpler way than was previously done; much of the inspiration for it comes from the work of Yamasaki (1968). It needs only ca. 1-1/2 hours on the CDC 6600 to predict one year.

Section 2 of this paper discusses the more important points of our earlier work which were conducive in preparing for the long-term model integrations done recently. Sections 3 and 4 describe the theoretical bases of respectively the air and sea portions of the present interaction model. Results of some three-year experiments with this combined model are presented in section 5. As overheating was evident in these experiments, other, shorter ones were made to demonstrate the control of surface temperature by adjusting such critical parameters as the surface drag coefficient and the vertical atmospheric diffusivity; these matters are also covered in section 5. A necessary comparison of the purely theoretical, computational findings with actual observations in the atmosphere and ocean, by both conventional and satellite techniques, appears in section 6.

## 2. Review of earlier work under this contract

Two experiments done with the old, ten-level air model along will be discussed first, followed by one example of a fully interacting computation. The initial wind field in this air model is geostrophic, zonal and non-divergent; initial temperatures, and therefore pressures, and relative humidities are annual Northern Hemisphere climatological means derived from M.I.T. General Circulation Project data; see Peixoto (1960) and Peixoto and Crisi (1965).

The following two cases are identical excepting their fixed surface temperature profiles. Figure 1 shows the initial surface _potential_ temperature profile for Case I, in which this temperature is constant within $14°$ latitude of the equator, but drops off at higher latitudes. The corresponding ordinary temperature profile, held constant in time, would show a small equatorial minimum about $0.3°C$ cooler than at latitude $14°$, on account of the surface pressure having an equatorial minimum. Directly above the potential temperature profile is the 12-day accumulated precipitation profile for this case. There is a sharp peak of 35 cm directly on the equator, indicating an active equatorial convergence zone. This rate of precipitation corresponds to about 1060 cm per year, three times the observed amount in the heart of the actual intertropical convergence zone at atoll stations like Funafuti; see Weather Bureau (1959). However, the actual ITCZ is seldom observed right on the equator, as will be shown in section 5 on satellite observations.

Figure 2 shows the evolution of the 9.6 km vertical motion profile for Case I; this altitude is very near the main level of non-divergence.
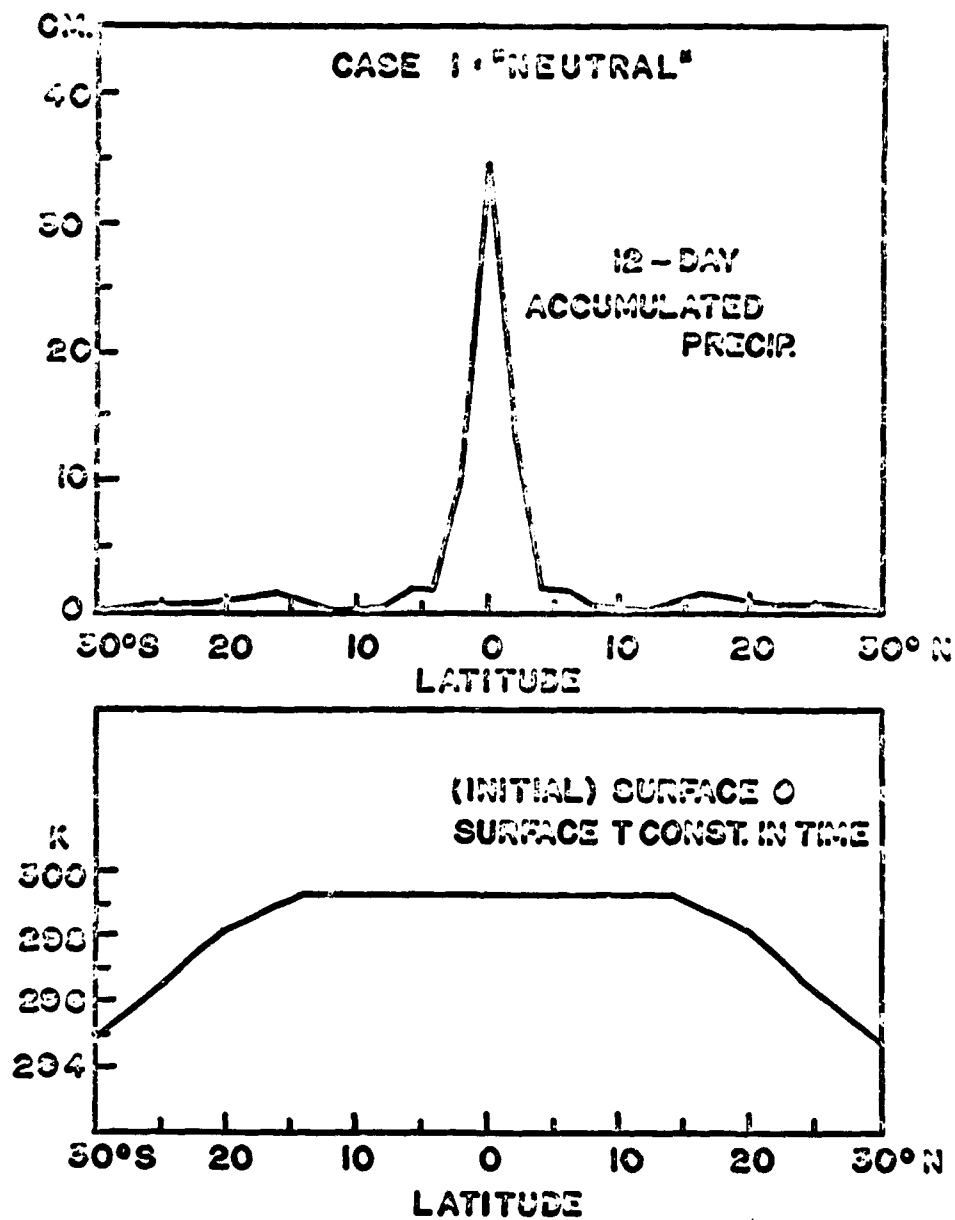
Fig. 1. Surface initial potential temperature and precipitation
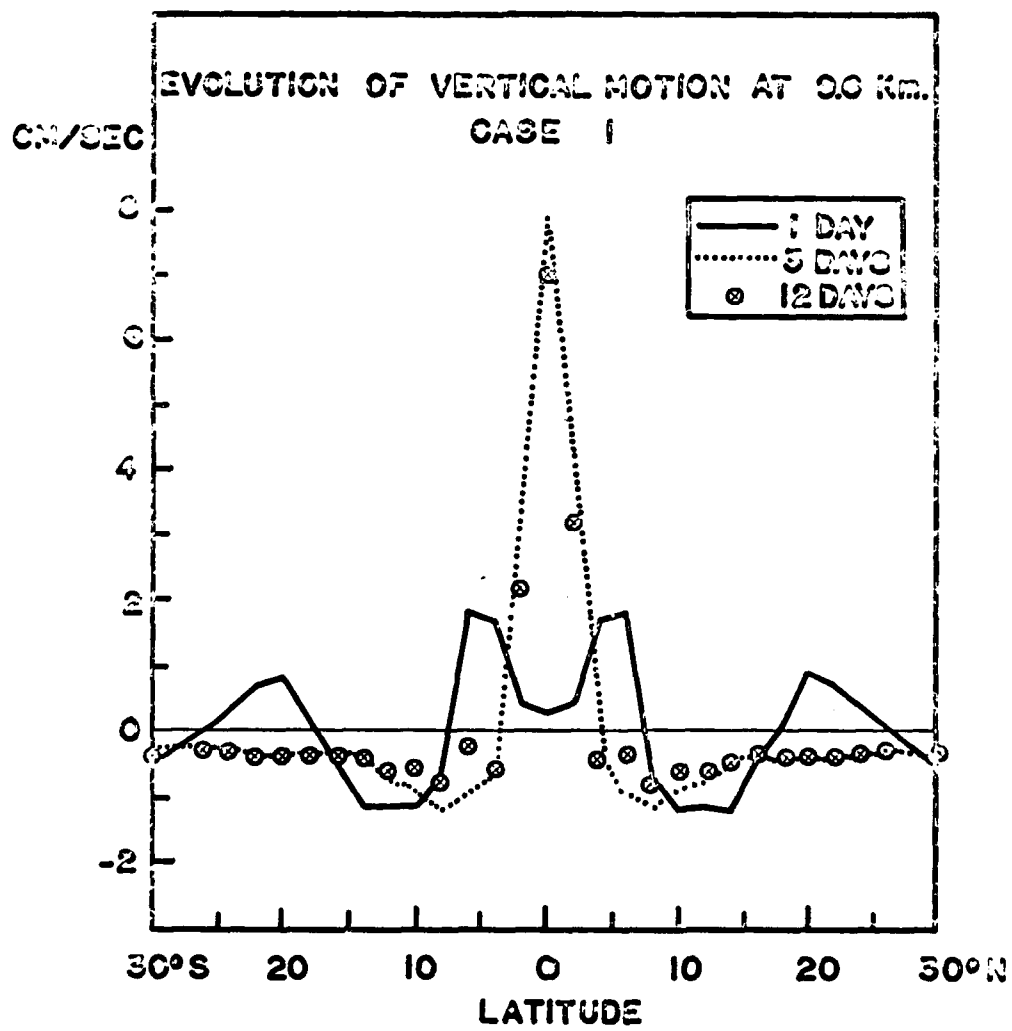profiles, "Neutral" case 1

Fig. 2. Evolution of vertical motion at 9.6 km, case I

At the initial time, of course, there is no vertical motion at all. One day later, as indicated by the solid line, a transient double updraft has developed at 6° South and North. There is thereafter a progressive consolidation of this double feature; by three days, as indicated by the dotted line, a pronounced single updraft is right on the equator. This single equatorial updraft appears to be very stable, as indicated by the vertical-motion profile at twelve days which is hardly different from that at three days. It is supposed that the initial transient double feature is induced by frictional convergence; the consolidation of it into a single updraft may well be aided by horizontal convergence of eddy heat flux from the two convection zones towards the equator. Once the single updraft has been established, its apparently great stability against physical and numerical perturbations prevents a breakdown into the double mode.

Before going on to Case II, it should be mentioned that the original work by Pike (1968) included an experiment carried out with a fixed surface temperature profile showing a definite maximum on the equator. The results were very similar to those for Case I, with a very small equatorial minimum, indicating that the qualitative structure of the ITCZ is not affected by this kind of temperature profile change.

In marked contrast to the above cases is Case II, where the surface temperature profile has a fixed double maximum off the equator at latitudes 8° South and North and a pronounced minimum on the equator. Figure 3 presents this new profile, similar in character to that which develops from cold equatorial upwelling and vertical mixing in the sea. Directly above the cold-equator temperature profile is drawn the corresponding 12-day accumulated precipitation profile. A double maximum off the equator, and directly over the latitudes of warmest surface water, is clearly indicated. Note that a marked hemispheric asymmetry in precipitation has developed despite the symmetric thermal forcing and other boundary conditions; this asymmetry has plainly been generated internally, probably by truncation error in solving a second-order differential equation for height-averaged pressure by marching, with successive approximations, in latitude from 30° South to 30° North; see section 3. Analytical details of this kind of pressure computation are given by Estoque and Bhumralkar (1969), section 4; the finite-difference scheme for solving the second-order equation is described in Richtmyer and Morton (1967), section 8.5. The mean of the two maxima is about 12 cm, corresponding to 365 cm per year, very close to the actually observed oceanic ITCZ precipitation rate peak.

The vertical motion profiles of Case II are shown in Figure 4. At one day, indicated by the solid line, the 9.6 km profile is very similar to the corresponding one for Case I. By three days, however, there is no indication of updraft consolidation; in fact, a modest equatorial downdraft is in evidence while the updrafts have moved to be over the warmest surface water. Influenced by above truncation error, one updraft has become much stronger than the other at 12 days while the equatorial downdraft persists; in this model the double ITCZ seems to be a metastable state analogous to a balanced seesaw that is
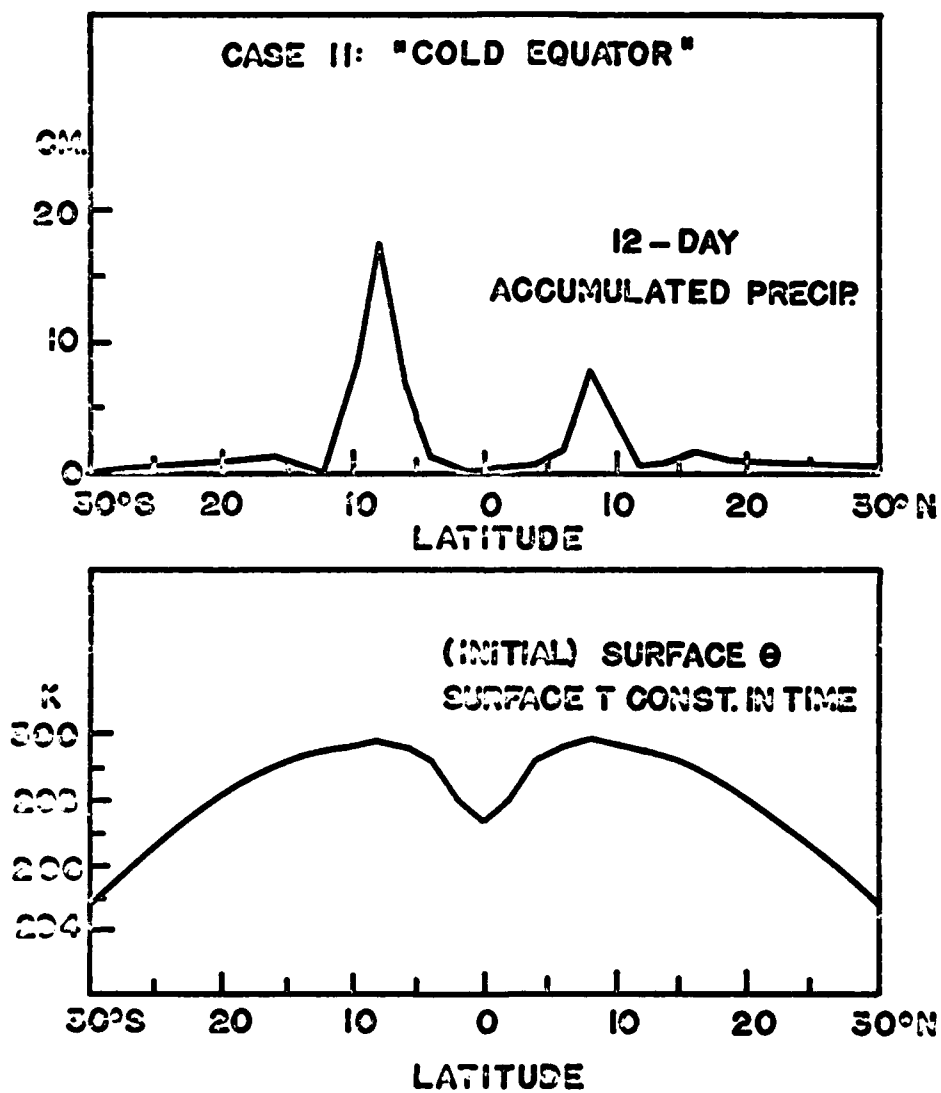
Fig. 3. Surface initial potential temperature and precipitation profiles, "Cold Equator" case II
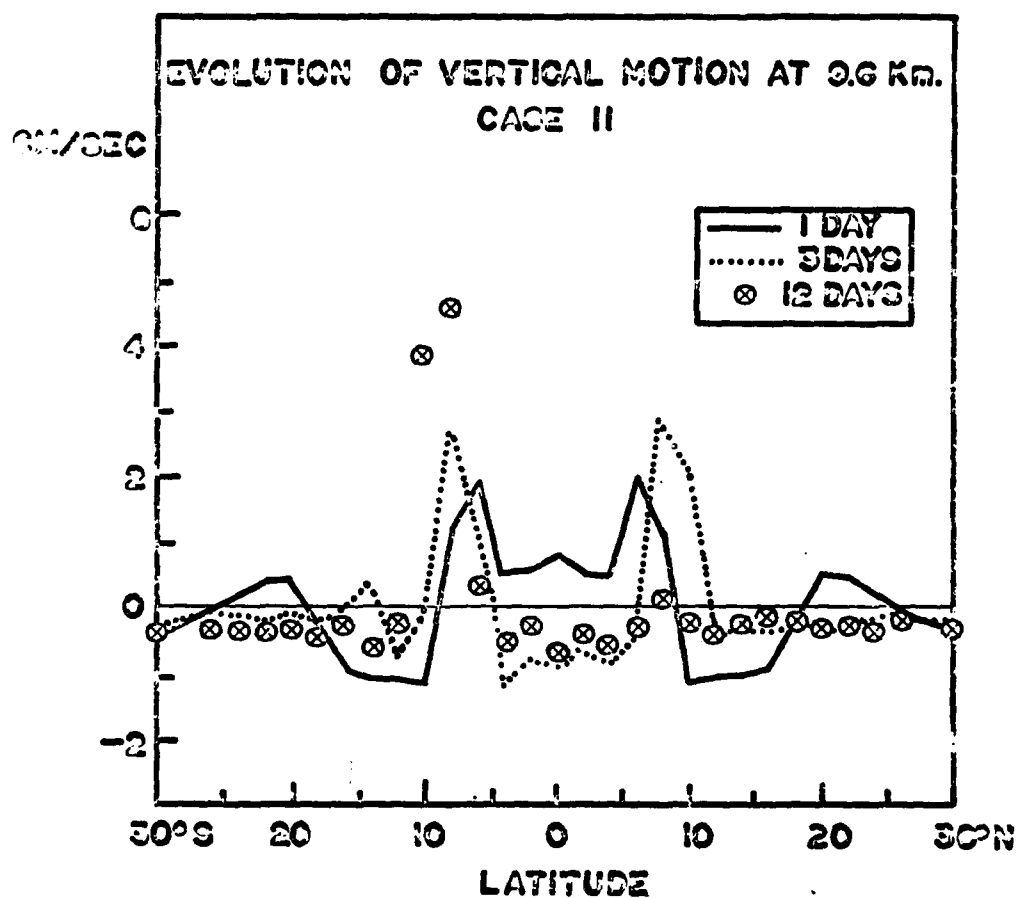
Fig. 4. Evolution of vertical motion at 9.6 km, case II

easily tipped into a more stable position with one end, or branch, pre-
dominant. It is supposed that the lack of updraft consolidation in Case
II is on account of equatorial surface cooling, which can counteract
the effect of horizontal eddy heat flux convergence. That the dominant
updraft formed in the southern, rather than more realistically in the
northern, hemisphere is a numerical accident; one cannot expect small
numerical perturbations in a meridional-plane model to have precisely
the same effect as real asymmetric forcing in a three-dimensional
atmosphere. The important point is that the model ITCZ prefers, as
does the real atmosphere's, a single mode; see Hubert et al. (1969).

Of the two cases presented, the second, with a marked sea surface
temperature minimum on the equator, appears to be the more realistic for
the open ocean, far from insular or continental influence; see Defant
(1961) for climatological maps of sea surface temperature.

In summary for the forced atmosphere model: experiments with it
so far suggest that ITCZ structure is intimately related to the meridional
surface temperature profile, at least over the sea. Given hemispherically-
symmetric conditions at the surface and in the subtropical atmospheric,
a single equatorial convergence zone appears to be the equilibrium state
unless there is a marked surface temperature minimum there, probably
caused by oceanic upwelling and vertical mixing. Then, as is usually
the case in the real atmosphere, the ITCZ will form several degrees of
latitude away from the cold equator; it may be double, with a branch
in each hemisphere, or, as is more likely, it will become single if one
of its branches reaches sufficient strength to suppress the other.

It was possible to combine the old air model with a sea model
similar to that described in section 4 to make a fully-interacting two-
fluid experiment. The 88 days of model time required about 7.5 hours
of computer time on the CDC 6600 at the National Center for Atmospheric
Research; horizontal grid spacing in the sea was the same as that in the
air as was the forward time step.

Some time after the completion of this experiment, two deviations
from the theory of section 4 were found in the computer code. Firstly,
the pressure gradient term $- \frac{\partial}{\partial x} (g'h)$ of equation (4.1) had been repre-
sented as $-g' \frac{\partial h}{\partial x}$ . Subsequent comparative tests of the sea model running
alone, forced by a typical surface stress profile derived from the data
of Hellerman (1967), showed only very small differences in the momentum,
depth and temperature profiles of the cases with differentiated and
undifferentiated g' . Secondly, the first coefficient of equation (4.15)
was set equal to 2 rather than 1/2, effectively doubling the value of
$k_o$ from 0.4 to 0.8. Subsequent tests with the forced sea model showed
that computed momentum, depth and temperature profiles were much more
realistic with the larger $k_o$; in fact, all that may accurately be said
about this particular constant is that it appears to be of order unity.
It appears, therefore, that the validity of our present experimental
results has not been significantly reduced by the above changes.

The initial latitudinal profiles of mixed-layer depth  h  and underlayer temperature  $T_o$  were given by

$$h(x) = 75 - 25\cos\left(\frac{\pi x}{x_{30}}\right) \text{ meters, and} \qquad (2.1)$$

$$T_o(x) = 15 + 5\cos\left(\frac{\pi}{2} \frac{x}{x_{30}}\right) \text{ deg.C} , \qquad (2.2)$$

where  $x_{30}$  is the value of the x co-ordinate at latitude 30° North. Expression (2.1) was chosen as a very rough first-order approximation to the observed Pacific thermocline data of Wyrtki (1964); expression (2.2), in conjunction with the other free parameters, seemed to influence the development of a realistic surface temperature profile, the initial form of which was identical to that in Case I of the forced air model - see figure 1. Of course, the above depth profile was allowed to vary in time while the above underlayer temperature profile was held constant. The initial surface current was zonal and geostrophic; as its maximum magnitude did not exceed two cm per sec, much less than what later developed, it is not shown in the following figures.

Unfortunately, a computer output tape covering the period of model time 11 through 48 days was lost during the two-fluid experiment; on account of economic considerations the computation coudl not be repeated, therefore, the detailed evolution of the model parameters cannot be discussed. However, it will be shown that the major features were changing only slowly at the end of the computation. Figure 5 shows the north-south profiles of zonal surface current, positive westward, at 49 and 88 days. By far the most important feature is a sharply peaked westward equatorial current; its top value of 65 cm/sec is just under 1.3 knots. It is clearly produced by the westward surface wind stress in low latitudes. The corrugated nature of this profile poleward of latitude 15° is a curious feature not readily explainable; it does not appear in any of our forced sea experiments. Not shown in figure 5 are two spurious westward currents that developed right at the lateral boundaries; these, too, did not appear in the forced sea model.

The profiles of meridional surface current in figure 6 are intimately related as effect to the zonal current and the meridional variation of Coriolis acceleration (beta affect) as cause. In both hemispheres this acceleration is poleward, and thus divergent, on a westward current centered at the equator; poleward current components are developed on both sides of the equator in this case. The surface horizontal divergence has a maximum of about $1.1 \times 10^{-6} \text{sec}^{-1}$ right on the equator; similar magnitudes of convergence occur at latitudes 3° South and North. Unfortunately, corrugations similar to those in the zonal current are present in the meridional component as well, as are spurious poleward components at the lateral boundaries at 88 days. This latter feature, not shown in the figure, lags behind its zonal
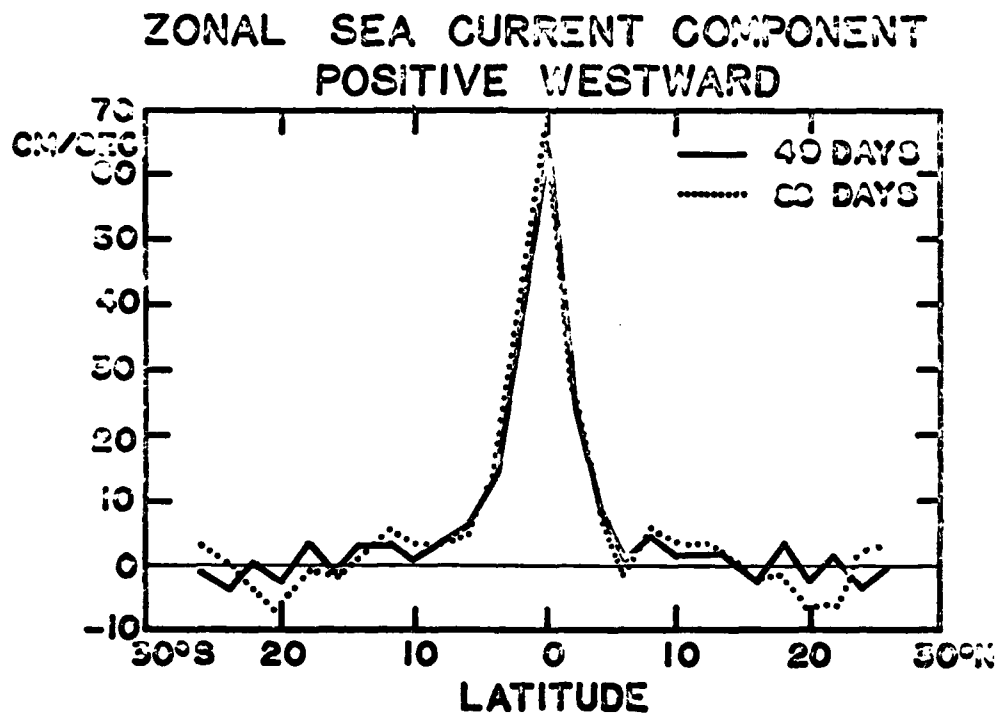
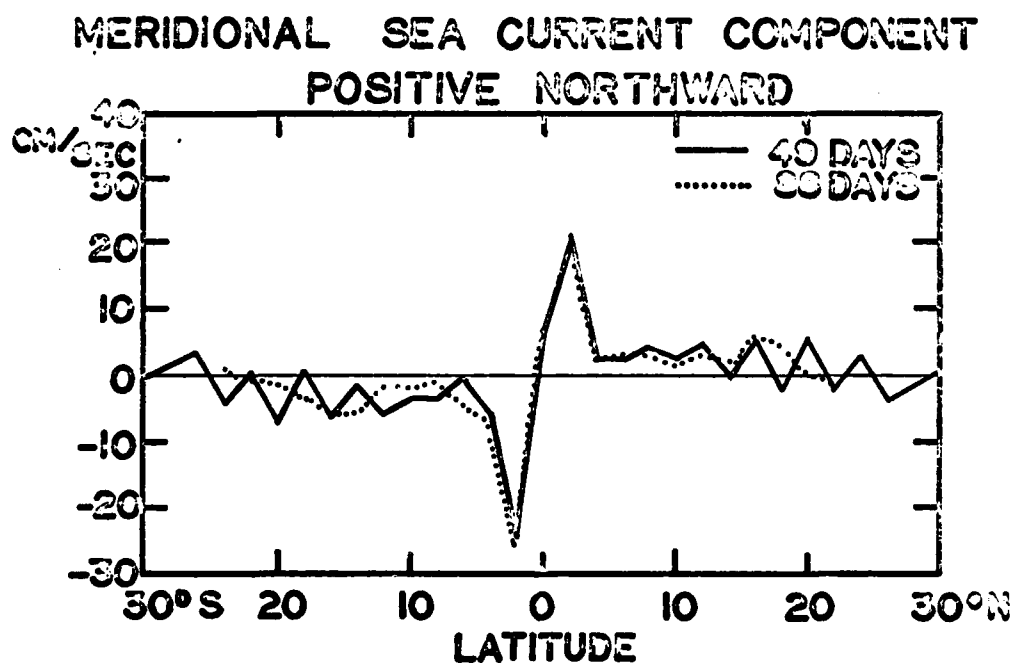Fig. 5. Zonal surface ocean current component, original
two-fluid case

MERIDIONAL SEA CURRENT COMPONENT
POSITIVE NORTHWARD



Fig. 6. Meridional surface ocean current component, original
two fluid case

counterpart in evolution and is certainly a secondary development pro-
duced by the Coriolis acceleration. None of these curiosities appeared
in the forced sea model.

Figure 7 shows the profiles of surface mixed layer depth at the
initial time and at 49 and 88 days. This profile's development is
obviously related to the divergence-convergence pattern implied by
figure 6; over the first 49 days the mixed layer has become shallower
in the equatorial region of horizontal divergence but deeper at higher
latitudes where surface convergence is the rule. On and very near the
equator, vigorous entrainment balances the strong divergence with the
maximum value of the parameter E, on the equator, reaching the order of
$10^{-3}$ cm/sec; our calculations show that E is relatively small or even
negative at two or more degrees of latitude off the equator. Between
49 and 88 days there is an insidious deepening of the mixed layer at all
latitudes; the active equatorial entrainment has not been completely
balanced by poleward mass transport. One basic problem is that a
meridional-plane model cannot include explicitly the mass removal effects
of a western boundary current.

Inclusion of a simple sea model in this investigation has as its
major objective the prediction of surface temperature; figure 8 presents
the results. When comparing this figure with earlier surface temperature
profiles, it should be recalled that the units of figure 8 are actual
temperature while those of the preceeding figures are potential temper-
ature; there is not much difference between the two at sea level. As
expected, the vigorous entrainment on the equator produces a marked
cooling of the sea surface there; this cooling slows down markedly but
does not stop completely during the later phase of the computation. The
maximum surface temperature is established at an average, over both
hemispheres, of latitude 8° and the average depression of temperature
from its maximum to the equatorial value is 3°C at 88 days. In fact,
the 88-day surface temperature profile predicted by the two-fluid ex-
periment is very similar to the fixed profile of Case II of the forced
air model; see figure 3. Admittedly, the interacting model does predict
almost one degree more equatorial cooling than desired and does not
behave very well at the lateral boundaries, showing unexpected warming
there, probably on account of the clear-sky solar radiation not decreasing
with latitude in this experiment.

However, the overall performance of our simple model in surface
temperature prediction has nicely revealed the expected equatorial
cooling. Since the atmospheric part is sensitive to only one variable,
the temperature, of the oceanic part, one may expect interesting and
realistic developments in the air model. Figure 9 shows the evolution
of atmospheric vertical motion at 9.6 km for the two-fluid case. There
is no such motion initially, but by one day the familiar double updraft
at 6° South and North latitude has developed just as in the forced air
cases. This feature merges to a single equatorial updraft by three
days; so far the model ITCZ is behaving generally as it did in Case I
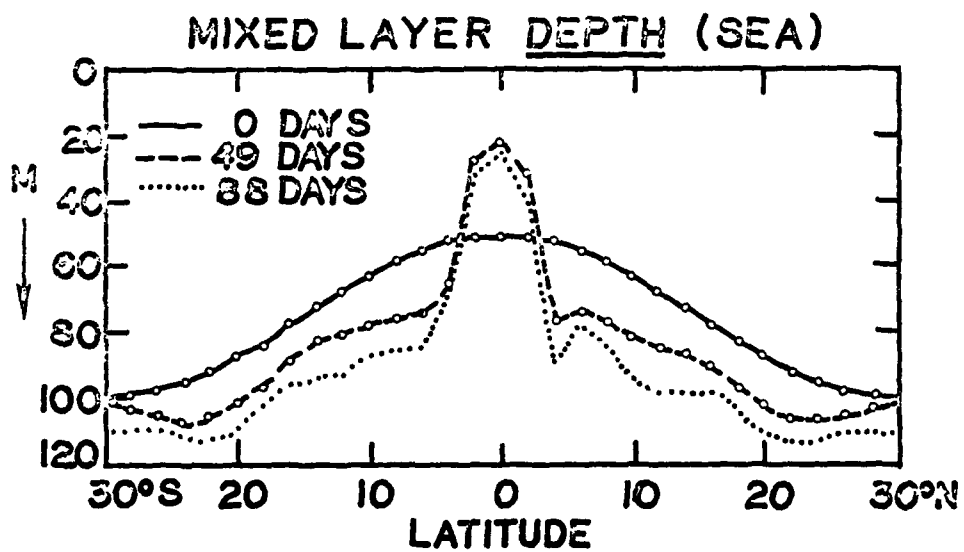of the forced air model with a flat surface temperature profile. By

Fig. 7.  Surface ocean mixed-layer depth, original two-fluid case
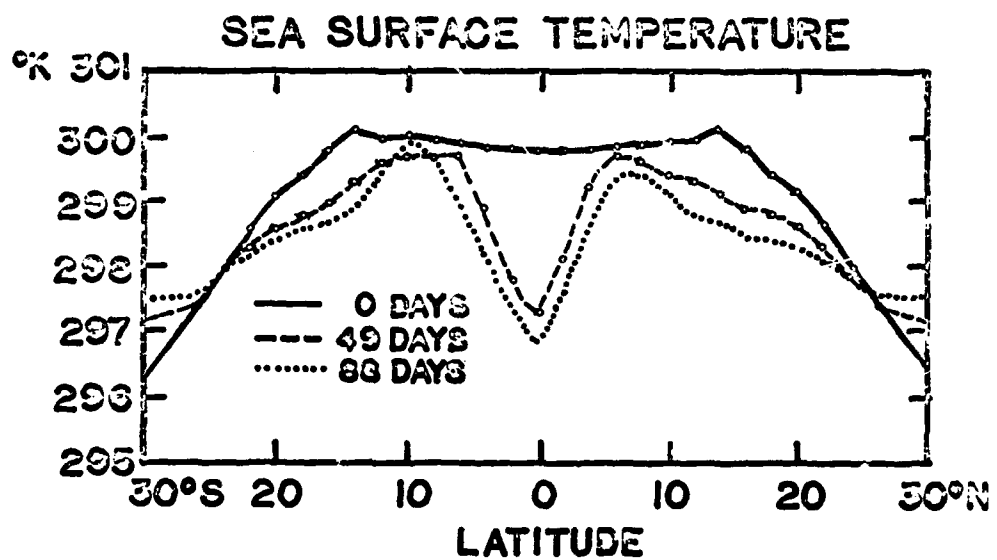
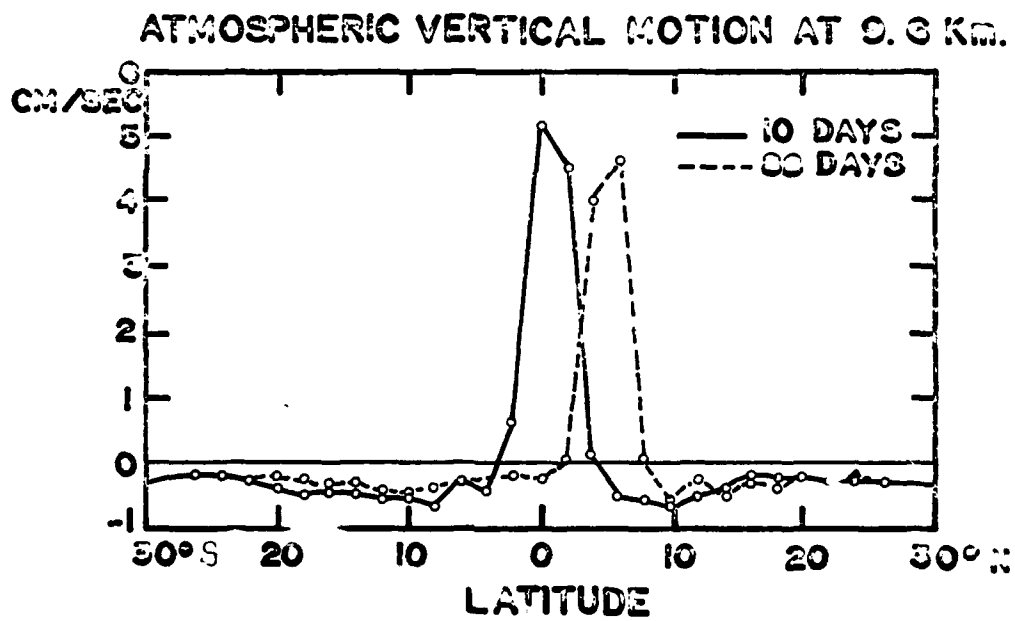Fig. 8. Surface temperature, original two-fluid case

ATMOSPHERIC VERTICAL MOTION AT 9.6 Km.

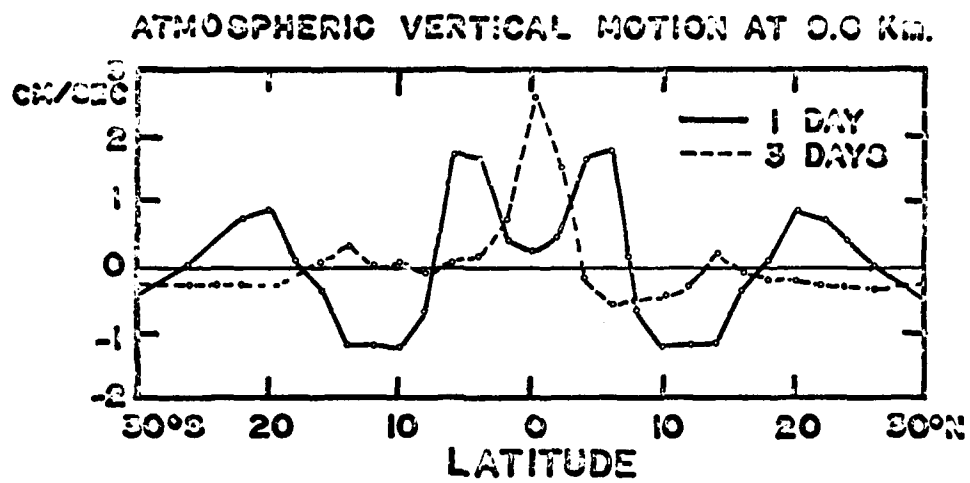

ATMOSPHERIC VERTICAL MOTION AT 9.6 Km.



Fig. 9. Evolution of atmospheric vertical motion at 9.6 km, original two-fluid case

ـ ـlays the ITCZ shows a tendency to start moving off the equator; at
this time equatorial surface cooling is still negligible. Thereafter,
as far as may be told from the incomplete computer output, the ITCZ
moves slowly but progressively poleward; by the end of the experiment
at 88 days it has reached latitude 6° North, directly over one of the
predicted surface temperature maxima. Obviously, the ITCZ seems to be
closely attached to the local heat source, both sensible and latent,
that a warm sea surface provides.

The gross evolution of the precipitation profile for this case is
seen in figure 10. Over the first nine days of the experiment, when
there is no pronounced dip in surface temperature at the equator, the
heaviest precipitation is centered no more than two degrees of latitude
away. Over the last nine days, though, the heaviest rainfall is located
with the maximum updraft over one of the well-defined temperature peaks
at latitude 6° North.

It is noteworthy that, as the equator cools, the model ITCZ does
not split into two parts, each one centered over a temperature maximum.
Instead, the single equatorial ITCZ at three days maintains its identity
while moving poleward, by chance towards the North, following the warm
water. It appears that the great stability of this well-developed fea-
ture prevents any breakdown into a double mode over the limited time
of the computation; note that in Case II of the forced air model the
intensification of one branch of a double ITCZ was accompanied by
weakening of the other branch. The single ITCZ, once formed, seems to
be very persistent, regardless of antecedent conditions. Truncation
error in the pressure computations probably accounts for the early,
small asymmetries which can grow with time. The physically meaningful
results accompanying the later, large asymmetries are the single nature
of the ITCZ and its location over a relatively warm surface; the par-
ticular hemisphere into which it moved is not significant in this particular
case.
Of course, the differences between hemispheres in the real atmosphere
are intimately related to three-dimensional effects accompanying the
distribution of land and sea. This simple model cannot include such
effects, but only suggest in a general way what form the zonally-averaged
ITCZ is likely to take in the presence of irregular perturbations.


3. A simple atmospheric model for long-term integrations

The air model is of a primitive-equation type and is constructed
in a meridional cross-section with Cartesian co-ordinates perpendicular
to a beta plane. Its domain is from latitude 30° South to latitude 30°
North and from sea level to the tropical tropopause just above 16 km.
The horizontal spacing of the finite-difference grid is two degrees of
latitude, except next to the lateral boundaries where it is four degrees.
Vertical grid levels are at 0 and 10 m and at 1.057, 5.870 and 16.535 km.
Space differencing is upstream for the advective terms but is centered
for all other terms such as the mass divergence and pressure gradient;
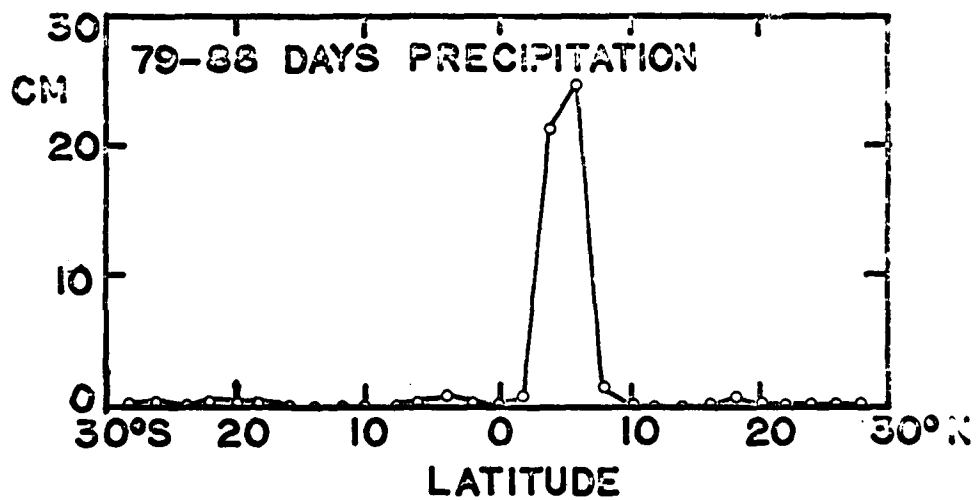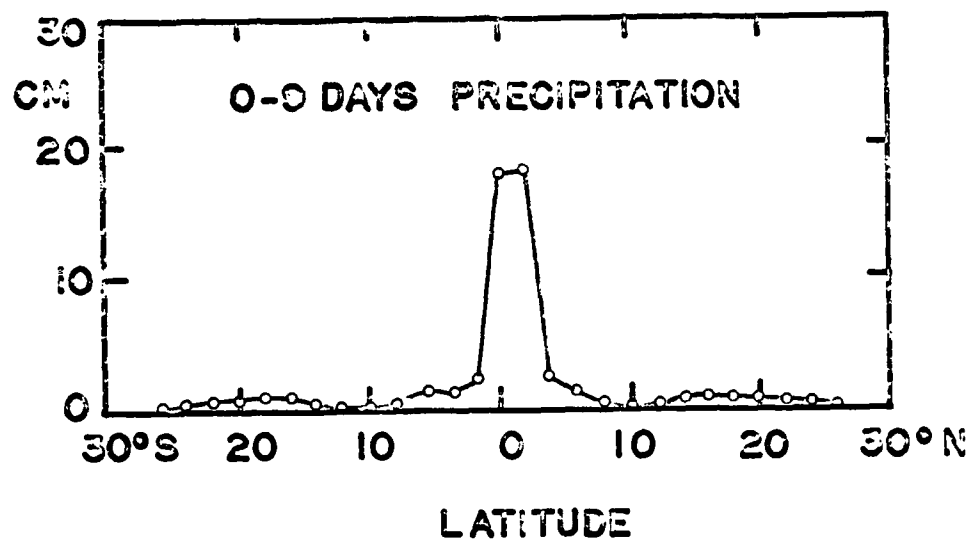
Fig. 10. Nine-day precipitation profiles, original two-fluid case

time differencing is forward with a step, Δt, of 30 minutes, the largest possible with reliable computational stability.

Four predictive equations are used: familiar momentum equations for the two horizontal velocity components, the first law of thermo-dynamics for the potential temperature and an equation of continuity for moisture. Vertical motion is computed from meridional motion using a steady-state approximation of the equation of mass continuity; the pressure field is obtained by assuming hydrostatic equilibrium. Explicitly, we have:

$$\frac{\partial u}{\partial t} = - u\frac{\partial u}{\partial x} - w\frac{\partial u}{\partial z} + fv - \frac{1}{\rho}\frac{\partial p}{\partial x} - \frac{1}{\rho}\frac{\partial F_u}{\partial z} + K_H\frac{\partial^2 u}{\partial x^2} \qquad (3.1)$$

$$\frac{\partial v}{\partial t} = - u\frac{\partial v}{\partial x} - w\frac{\partial u}{\partial z} - fu - \frac{1}{\rho}\frac{\partial F_v}{\partial z} + K_H\frac{\partial^2 v}{\partial x^2} \qquad (3.2)$$

$$\frac{\partial \theta}{\partial t} = - u\frac{\partial \theta}{\partial x} - w\frac{\partial \theta}{\partial z} + Q_L + Q_C + Q_R - \frac{1}{\rho}\frac{\partial F_\theta}{\partial z} + K_H\frac{\partial^2 \theta}{\partial x^2} \qquad (3.3)$$

$$\frac{\partial q}{\partial t} = - u\frac{\partial q}{\partial x} - w\frac{\partial q}{\partial z} + S_q - \frac{1}{\rho}\frac{\partial F_q}{\partial z} + K_H\frac{\partial^2 q}{\partial x^2} \qquad (3.4)$$

$$\frac{\partial}{\partial x}(\rho u) + \frac{\partial}{\partial z}(\rho w) = 0 \qquad (3.5)$$

$$\frac{\partial}{\partial z}\left(\frac{p}{p_o}\right)^\kappa = - \frac{g}{c_p\theta} \qquad (3.6)$$

Here, x represents a northward directed co-ordinate and z the vertical co-ordinate. u and v are respectively the northward and westward wind velocity components; w is the vertical velocity component. f is the Coriolis parameter, zero on the equator and varying linearly with x according to a constant beta parameter of $2.19 \times 10^{-13} cm^{-1} sec^{-1}$. The latent heat of condensation for water is denoted by L while ρ is the density, computed from initial data by the equation of state (3.7) and held constant in time. The acceleration of gravity is denoted by g .

$$\rho = \frac{p_o^\kappa p^{1-\kappa}}{R\theta} \qquad (3.7)$$

$p_0$ is the standard reference pressure of 1000 mb, p is variable pressure, $\theta$ stands for potential temperature, R is the specific gas constant for dry air, and $\kappa \equiv R/c_p$ where $c_p$ is the specific heat of dry air. Note that the effect of moisture on air density has been neglected.

$F_u$, $F_v$, $F_\theta$ and $F_q$ are respectively the vertical turbulent fluxes of specific momentum, sensible heat plus potential energy in terms of potential temperature, and moisture in terms of mixing ratio q . We shall consider them to be positive upward. At the surface these fluxes are computed by the bulk transfer formula

$$F_s = (\rho c_D U)_{10} (s_0 - s_{10}) \qquad (3.8)$$

where s may be either u, v, $\theta$ or q . $c_D$ is the surface drag coefficient and U is the total horizontal wind speed. The subscripts 0 and 10 indicate values taken at the 0m and 10m levels respectively. In the interior of the model, an Austausch formula is used to compute these fluxes:

$$F_s = - \rho K_z \frac{\partial s}{\partial z} \qquad (3.9)$$

where $K_z$ is the constant vertical diffusivity. At the topmost model level, vertical fluxes are not computed and their vertical gradient terms in the predictive equations are neglected.

$Q_C$ represents the condensation heat source associated with atmospheric convection. We have modelled this very important process in a manner similar to that of Yamasaki (1968), assuming that convective latent heat release is directly proportional to the mean upward moisture flux, $\overline{F}_q \equiv \frac{\rho(w+|w|)q}{2}$ . Convective heating in our model may occur only at the 1.057 and 5.870 km levels, denoted respectively by the subscripts b and a; $Q_C$ is always zero elsewhere. Specifically,

$$Q_{Cb} = \frac{L}{c_p (\rho \Delta z)_b} (\frac{p_0}{p_b})^\kappa \overline{F}_{qb} \ell$$

$$\qquad (3.10)$$

$$Q_{Ca} = \frac{L}{c_p (\rho \Delta z)_a} (\frac{p_0}{p_a})^\kappa [\overline{F}_{qb}(1-\ell) + \overline{F}_{qa}]$$

The mass per unit area between the level in question and that next above it is given by $\rho \Delta z$ . The fraction of the upward moisture flux through the lower level, subscript b , assumed to condense between levels b and a is symbolized by $\ell$ .

The latent heat release on account of large-scale condensation in the presence of super-saturation is given by $Q_L$, where

$$Q_L = \frac{L}{c_p} \left(\frac{p_o}{p}\right)^\kappa \frac{[(q-q_s) + |q-q_s|]}{2\Delta t} \quad . \tag{3.11}$$

Here, $q_s$ is the saturation specific humidity and $\Delta t$ is the computational time step.

In any atmospheric model designed for integrations over many weeks of physical time, a radiational heat sink, $Q_R$, is necessary. It may be expressed as

$$Q_R = \left(\frac{p_o}{p}\right)^\kappa \left(\frac{\partial T}{\partial t}\right)_R \tag{3.12}$$

where $\left(\frac{\partial T}{\partial t}\right)_R$ is the local rate of change of temperature on account of all radiational effects. This rate of change may either be specified, say as a function of height only from the data of Smagorinsky et al. (1965), or computed. See section 5 for an example of such a computation.

An atmospheric moisture sink, $S_q$, accompanying the condensation process is included in the moisture continuity equation. It is expressed by

$$S_q = \frac{(q_s-q) - |q-q_s|}{2\Delta t} + w \frac{\partial q}{\partial z} s(Q_c) \tag{3.13}$$

where $s(x) = 0$ for $x \leq 0$ and $s(x) = 1$ for $x > 0$. The first term represents the falling out of moisture associated with large-scale condensation heating $Q_L$ while the second term indicates that all moisture advected upward in the presence of convectional heating $Q_c$ is removed from the atmosphere. Note that liquid water storage by clouds is neglected in this model.

The specification of horizontal turbulent mixing by the simplest method possible, using a constant horizontal diffusivity $K_H$, completes the model's basic set of equations.

Determination of the vertical motion field requires vertical integration of equation (3.5) from the surface, where $w = o$ is assumed, to the top of the model; since this level, H, is about at the tropical tropopause, the vertical motion is set to zero there too. This state is realized by requiring the total meridional mass transport,

$\int_o^H \rho u dz$, to vanish everywhere; the final meridional velocity component

u is obtained from the computed value $u_c$ by the correction equation

$$u(z) = u_c(z) - \frac{\int_0^H \rho u_c dz}{\int_0^H \rho dz} . \tag{3.14}$$

The pressure field is obtained by downward integration of equation (3.6) from the model top to the surface; the pressure at the top, a function of latitude and time, is computed as in Estoque and Bhumralkar (1969), section 4.

The boundary conditions of this model are relatively simple. On the lateral boundaries at latitudes 30 South and North, u, v, θ and q are specified as functions of height and time; the boundary pressure profile is computed at each time step by assuming a fixed surface pressure and then integrating upward hydrostatically to the model top. Vertical motion is set to zero at these latitudes. At the surface, all momentum components are assumed to vanish, the potential temperature corresponds to the temperature computed by the sea model described in section 4 and the specific humidity is set to its saturation value. On the top boundary all the predictive equations (3.1) through (3.4) are applied, but there are assumed to be no vertical motion or advection, no vertical flux gradients, no convective heating and no corresponding moisture sink.

## 4. A compatible oceanic model

Our simple sea model for the prediction of surface temperature approximates the real ocean by assuming an active surface mixed layer of variable depth h overlying an inert lower layer of infinite depth. As in the model of Kraus and Turner (1967), the real thermocline of finite thickness is replaced by an abrupt decrease in sea temperature from the mixed-layer value $T_s$ to the lower underlayer value $T_o$, occurring at depth h . As in the air model, the predictive equations are primitive in form with only one horizontal dimension - that of latitude. They are four in number, predicting the northward component of surface current, $u_s$ and the westward component of surface current, $v_s$, as well as $T_s$ and h . The $u_s$ and $v_s$ equations are in momentum form, the $T_s$ equation is a form of the first law of thermodynamics for an incompressible fluid and the h equation is an equation of continuity. Explicitly, we have

$$\frac{\partial u_s}{\partial t} = - u_s\frac{\partial u_s}{\partial x} - \frac{E^* u_s}{h} - \frac{F_{us}}{\rho_s h} - \frac{\partial}{\partial x}(g'h) + fv_s + \frac{1}{h}\frac{\partial}{\partial x}(Kh\frac{\partial u_s}{\partial x}) \tag{4.1}$$

$$\frac{\partial v_s}{\partial t} = - u_s \frac{\partial v_s}{\partial x} - \frac{E^* v_s}{h} - \frac{F_{vs}}{\rho_s h} \qquad - f u_s + \frac{1}{h} \frac{\partial}{\partial x} (Kh \frac{\partial v_s}{\partial x}) \qquad (4.2)$$

$$\frac{\partial T_s}{\partial t} = - u_s \frac{\partial T_s}{\partial x} - \frac{E^*(T_s - T_o)}{h} + \frac{S}{h} \qquad + \frac{1}{h} \frac{\partial}{\partial x} (Kh \frac{\partial T_s}{\partial x}) \qquad (4.3)$$

$$\frac{\partial h}{\partial t} = - u_s \frac{\partial h}{\partial x} - h \frac{\partial u_s}{\partial x} + E \qquad + \frac{\partial}{\partial x} (K \frac{\partial h}{\partial x}) \qquad (4.4)$$

It has been tacitly assumed that, for the lower layer, $u_o = v_o = 0$ and $h_o = \infty$ . Time differencing is forward with the same step as in the air model; space differencing is upstream, also as in the air model. The sea density, $\rho_s$, is assumed to be 1 gm $cm^{-3}$; $-F_{us}$ and $-F_{vs}$ are respectively the northward and westward components of the surface wind stress, computed by the air model. The reduced gravity, $g'$, is computed by

$$g' = g\alpha(T_s - T_o) \quad , \qquad (4.5)$$

where $\alpha$ , taken as 2.1 x $10^{-4}{}^oK^{-1}$ , is the thermal expansion coefficient of water at 20°C. zero salinity and one atmosphere pressure. The net downward heat flux at the sea surface, S , is obtained by the expression

$$S = \frac{R\downarrow - \epsilon\sigma T_s^4 - c_p (\frac{p_s}{p_o})^\kappa F_{\theta s} - L F_{qs}}{\rho_s c} \qquad (4.6)$$

where $c = 1$ cal $gm^{-1o}K^{-1}$ is the specific heat of water, $\sigma = 1.355$ x $10^{-12}$ cal $cm^{-2}sec^{-1o}K^{-4}$ is the Stefan-Boltzman constant $p_s$ is the surface pressure, and $F_{\theta s}$ and $F_{qs}$ are respectively the surface values of $F_\theta$ and $F_q$ as computed by the air model. The downward short-wave radiative flux $R\downarrow$ and the net long-wave emissivity $\epsilon$ are obtained by

$$R\downarrow = 0.94(1 - 0.68n) R_o \qquad \text{and} \qquad (4.7)$$

$$\epsilon = 0.985(0.39 - 0.05\sqrt{e})(1 - 0.6n^2) \quad . \qquad (4.8)$$

Here, $R_o$ is the seasonally-variable average daily clear-sky short wave radiation flux, obtained from the approximate expression (4.9) where

$R_{oo} = 7.95 \times 10^{-3} cal\ cm^{-2} sec^{-1}$ is the equatorial equinoctial value of $R_o$, obtained from Budyko (1956).

$$R_o = R_{oo}(\frac{\pi}{2} \sin\phi \sin\delta + \cos\phi \cos\delta) \tag{4.9}$$

The latitude is denoted by $\phi$ while the solar declination $\delta$ is computed by

$$\delta = 23.45° \sin 2\pi(\frac{t + t_p}{t_y}) \tag{4.10}$$

where $t_p$ is a thermal lag time and $t_y$ is the length of one year. e is the vapor pressure in millibars of the air at the 10 m level, obtained from the air model; and n is the cloudiness of the sky in tenths. Using data from the air model, we have computed n according to the formula

$$q_r \equiv \frac{1}{H} \int_o^H (\frac{q}{q_s})dz$$

$$n = 0\ 0 \quad if \quad q_r \leq 0.2$$

$$n = (q_r - 0.2)/0.6 \quad if \quad 0.2 < q_r < 0.8 \tag{4.11}$$

$$n = 1.0 \quad if \quad q_r \geq 0.8$$

Expressions (4.7) and (4.8) are taken from Kraus and Rooth (1961). Note that S has the dimensions [velocity x temperature].

Further, we have the entrainment parameter E of dimensions [velocity]; this variable represents the entrainment of underlayer water into the surface mixed layer with resulting modification of this upper layer by vertical mixing; it is computed by

$$E = \frac{C_E U_*^3 + C_E'(u_s^2 + v_s^2)^{\frac{3}{2}}}{g'h} - \frac{S}{T_s - T_o} \tag{4.12}$$

Here, $U_*$ is the surface friction velocity with respect to <u>water</u> density, obtained by

$$U_* = \left[\frac{(\rho C_D)_{10}}{\rho_s}\right]^{1/2} U_{10} \tag{4.13}$$

$C_E$ = 5.0 is an empirically-determined constant coefficient, derived from Turner (1969), allowing some of the downward surface turbulent kinetic energy flux to assist the mixing process at the thermocline and $C_E'$ = 1.0 x 10$^{-5}$ is a similar coefficient representing the part of the mixing process associated with vertical current shear. This value of $C_E'$ was chosen so that the wind-stress and current-shear contributions to mixing would be of approximately equal magnitude in equatorial latitudes. Note that the surface heat flux S is made to reduce the thermocline mixing in the sense that downward heat flux tends by itself to establish a shallower, and warmer, surface mixed layer. It S should become sufficiently large to make E negative, a reformation of the surface layer at shallower h is indicated; in this circumstance there is effectively no mixing of momentum or heat across the thermocline. Therefore, E is replaced by E* in the momentum and temperature equations where

$$E^* = \begin{array}{l} E \text{ if } E \geq 0 \\ 0 \text{ if } E < 0 \end{array} \qquad (4.14)$$

Lastly, K is the horizontal diffusivity; in this sea model it has been found that the variable form discussed by Smagorinsky et al. (1965), p. 730, helps to establish a realistic latitudinal profile of surface temperature. For one horizontal dimension only, this particular diffusivity is expressed by

$$K = \frac{1}{2} (k_o \Delta x)^2 \left[ \left(\frac{\partial u_s}{\partial x}\right)^2 + \left(\frac{\partial v_s}{\partial x}\right)^2 \right]^{\frac{1}{2}} , \qquad (4.15)$$

where $k_o$ is an empirical coefficient supposed by Smagorinsky to be equal to von Karman's constant, 0.40, and $\Delta x$ is the horizontal grid spacing. Note that the horizontal diffusion terms in the momentum and heat equations are conservative of the vertically-integrated momentum components $\rho u h$ and $\rho v h$ and of the vertically-integrated enthalpy $\rho c T h$ , redistributing them only. In contrast, the "horizontal diffusion" term

$$\frac{\partial}{\partial x} \left( K \frac{\partial h}{\partial x} \right) = \frac{1}{h} \frac{\partial}{\partial x} \left( K h \frac{\partial h}{\partial x} \right) - \frac{K}{h} \left(\frac{\partial h}{\partial x}\right)^2 \qquad (4.16)$$

is dissipative of the integrated potential energy $\rho g h^2$ on account of the negative-definite part in $\left(\frac{\partial h}{\partial x}\right)^2$ ; this somewhat unusual term in the continuity equation represents mass mixing by meridional-plane eddies at the bottom of the surface layer in analogy to mixing by horizontal-plane eddies at the edge of fast currents such as the Gulf Stream; see Stommel (1966). p. 54. Without it, uncontrolled deepening of the surface layer in regions of persistent horizontal convergence would occur in our model, as has been verified by numerical experiment.

## 5. Results of long-term integrations with the new combined air-sea model

Ideally, a combined atmosphere and ocean model should be computed over a period of physical time long enough to reach statistical equilibrium in the sea. However, since this period is of the order of 100 years (Manabe and Bryan, 1969), the ca. 150 hours of CDC 6600 time needed for such an experiment with our in-tandem model is impractically large. The seasonally-variable solar heating to be used cast doubts on utilizing Manabe and Bryan's procedure of marching forward the sea model many times faster than the air model, effectively computing with a much longer time scale in the sea. It was decided that the time scale of interest in our experiments was the one-year period of the heating cycle rather than the much longer thermal relaxation time of the sea. For our purposes, then, adequate adjustment in the sea would be signalled by the low-latitude surface temperature undergoing one-year fluctuations, at constant lag with respect to the solar forcing.

Two three-year experiments were made with the new, simple and efficient interacting model; they differed only in the initial and boundary conditions. In the air: using the atmospheric climatological data of Kidson et al. (1969), two sets of such conditions were set up: one with the mean of real Northern and Southern hemisphere zonally-averaged data being used in both model hemispheres, and the other with each real hemisphere's data in the corresponding model hemisphere. The former case may be called initially symmetric while the latter case was initially asymmetric. Both sets of initial conditions represented annual means in the interior and on the boundaries; both sets of lateral boundary conditions, at latitudes 30 North and South, consisted of variables fluctuating sinusoidally about their annual means with a period of one year and with amplitudes according to climatology. In the sea: both the symmetric and the asymmetric initial surface temperature profiles were obtained from Wyrtki's (1964) data at longitude 140°W, in the east-central Pacific, modified to eliminate the observed equatorial cool zone. In the three-year experiments all the oceanic predictive equations were applied at the lateral boundaries, assuming zero gradients of the predicted properties poleward of these boundaries.

In the atmospheric model, the initial pressure field was obtained from the initial potential temperature field by prescribing in all cases an initially hemispherically symmetric surface pressure profile

$$p_s(x) = 1015\text{mb} - 5\text{mb}\cdot\cos\left(\frac{\pi x}{x_{30}}\right) \qquad (5.1)$$

and then integrating the hydrostatic equation (3.5) upward. The initial wind field was computed from the resulting pressure field by assuming it to be zonal, geostrophic, horizontal and non-divergent. Initial specific humidities were computed by assuming the initial relative humidity to be a function of height only and to be equal to the values given by Jordan (1958) for the annual mean tropical atmosphere. In the oceanic model, the initial mixed-layer depth and underlayer temperature profiles were given by equations (2.1) and (2.2); the initial current

was obtained by using the same assumptions made for the initial atmospheric winds.

The following values of the various adjustable atmospheric constants were used in both three-year experiments: surface drag coefficient $C_D = 1.0 \times 10^{-3}$; vertical atmospheric diffusivity $K_z = 2 \times 10^{-4} cm^2/sec$; moisture condensation fraction $\ell = 0.34$ - Yamasaki's (1968) value for our vertical grid levels in a mean tropical atmosphere; horizontal atmospheric diffusivity $K_H = 10^{10} cm^2/sec$ - from Murgatroyd (1969). The radiational cooling $(\frac{\partial T}{\partial t})_R$ in equation (3.12) was taken as -0.45 C/day at the 0.010, 1.057 and 5.870 km levels and zero elsewhere. The initial thermal lag time $t_p$ was set at eight weeks and the length of one year $t_y$ was assumed to be 52 weeks. In the sea model, the horizontal mixing coefficient $k_o$ was put at 0.30 as in our earlier work.

Very similar results were obtained from the initially symmetric and the initially asymmetric cases. Figure 11 shows the superimposed three-year accumulated precipitation profiles for both cases; there is hardly any difference between them except for minor variations which may be ascribed mostly to numerical errors. Note the two well-defined precipitation peaks at latitudes 6N and 8S separated by a well-marked equatorial minimum; these two maxima and the minimum are intimately associated with respectively the warm sub-equatorial and the cold equatorial sea surface temperatures all our interacting model experiments predict; see fig. 13.

On account of the basic similarity between the two three-year cases, further discussion of them will be limited to the initially symmetric experiment. It is apparent that hemispheric asymmetries in the real atmosphere are essentially three-dimensional, with the different distributions of land and sea influencing the different atmospheric eddy characteristics of the two hemispheres which in turn influence the different zonal-mean structures; see Dickinson (1970). The relative simplicity of our model, restricted as it is to meridional-plane dynamics with no zonal-meridional eddy correlations, suggests that its results be presented at least as much in their own right as in comparison to the real atmosphere.

The quasi-symmetrical rainfall profiles of figure 11 should not be interpreted as being produced by a double ITCZ of approximately equal strength in both hemispheres at any one time. Instead, the double precipitation peak has been caused by a single ITCZ which establishes itself over the surface temperature maximum in the warmer hemisphere and migrates quickly across the cool equator into the opposite hemisphere whenever the progress of the seasons causes the hemispheric thermal asymmetry to reverse. Figure 12 shows the maximum surface temperature in the sub-equatorial warm water zone, five to ten degrees latitude, of each hemisphere as a function of time; note that the seasonal variation becomes very clear and that the two hemispheres are nicely out of phase. The lag of each hemisphere's maximum sub-equatorial temperature behind the corresponding summer solstice is
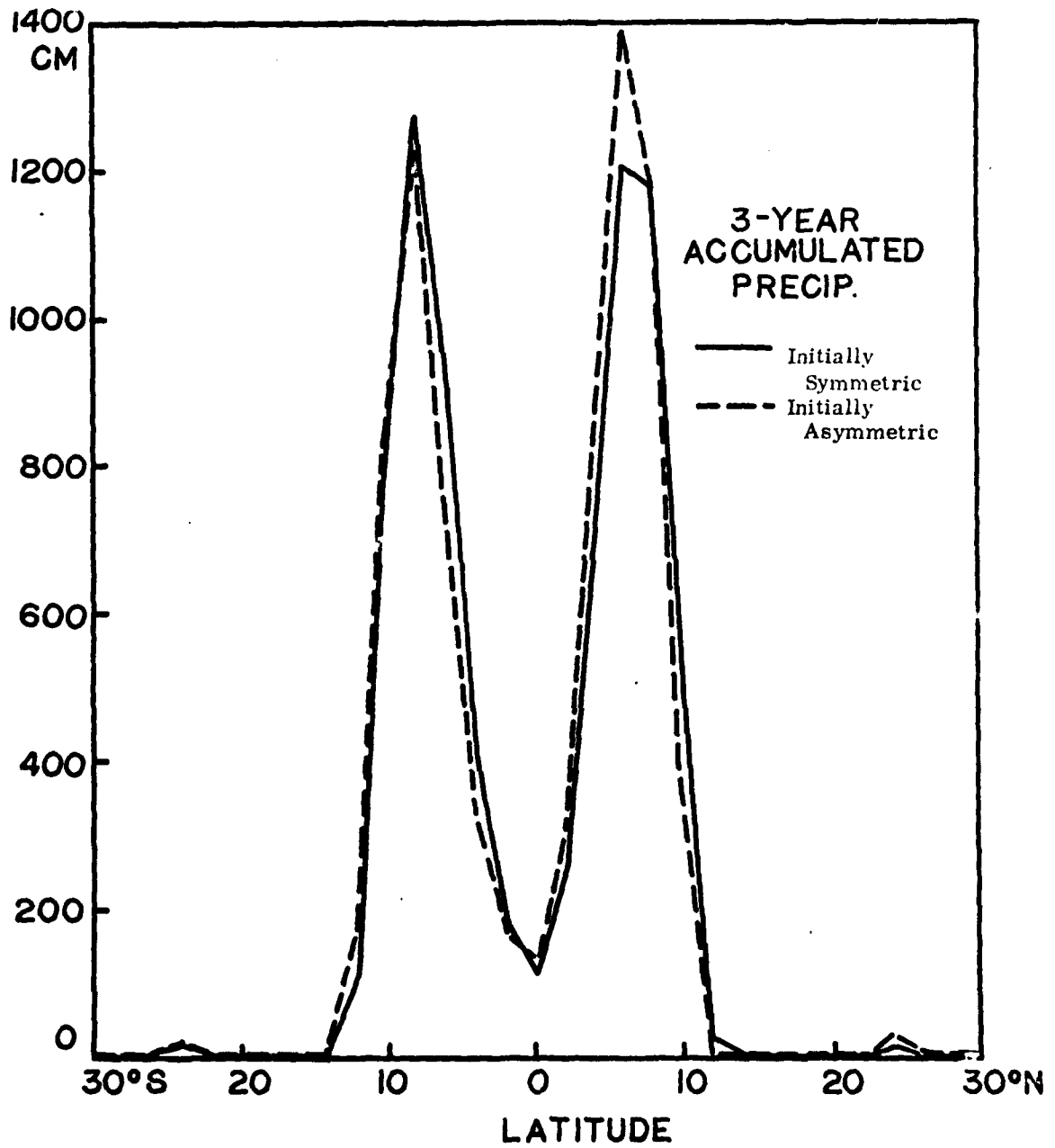
Fig. 11: Three-year precipitation profiles, long-term interacting experiments
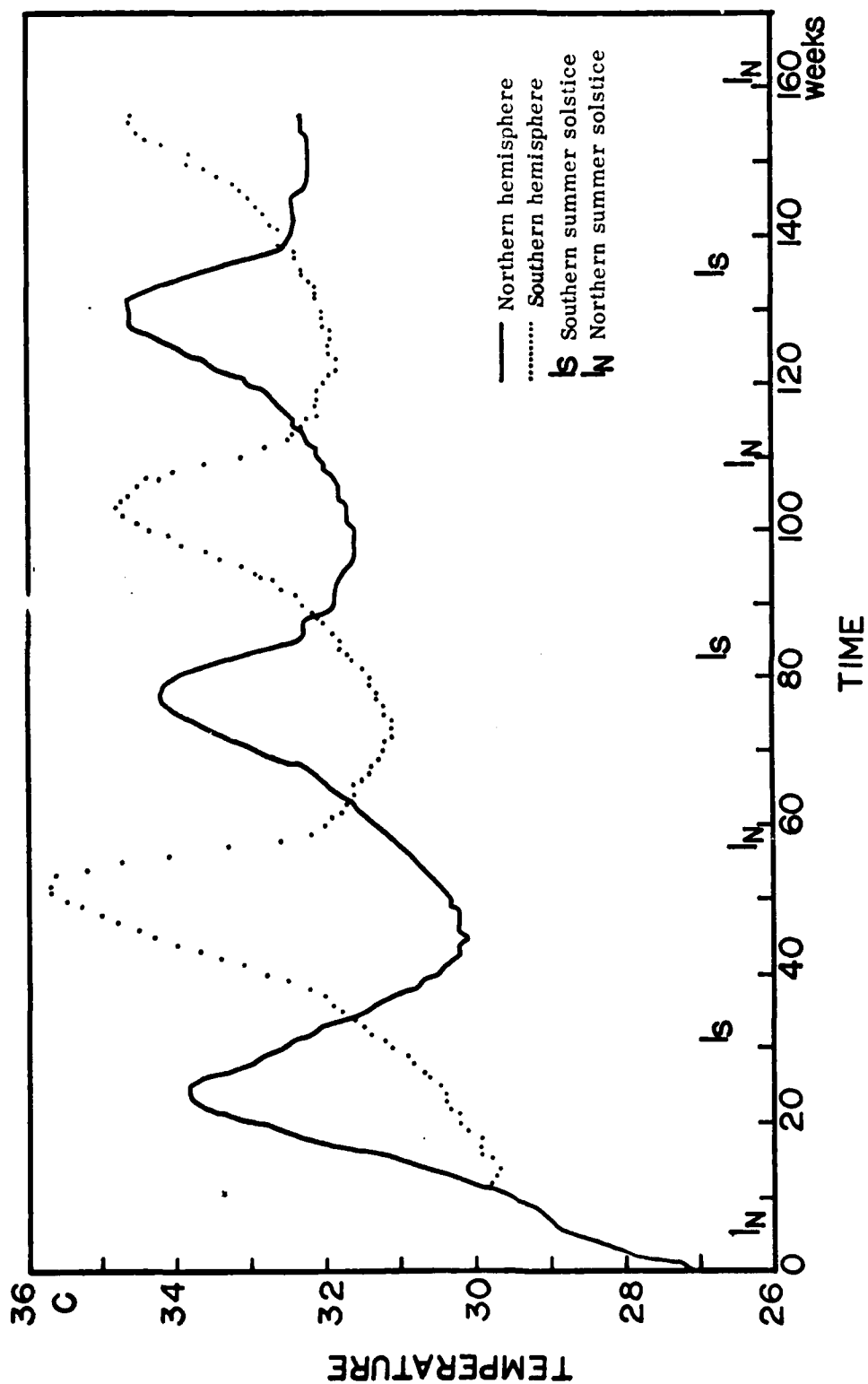
Fig. 12: Seasonal variation of maximum sub-equatorial surface temperature. both
hemispheres. initially symmetric experiment.

computed to be 20 weeks; since the overhead sun of late summer occurs
at these latitudes about eleven weeks after this solstice, the oceanic
thermal lag behind the maximum solar heating of late summer is about
nine weeks, or two months - a reasonable value. Apparently the relatively
small decrease of solar heating which follows the overhead sun of early
spring is not sufficient to force a double maximum, in time, of the low-
latitude sea surface temperature; the ocean's large thermal lag tends
to smooth the temperature (time) curve to show only one maximum each
year, at least in our model.

Note that the computed surface temperatures in this three-year
experiment rise to be about five degrees C above the initial, climato-
logical value. Some possible reasons for such excessive warming will
be discussed later in this section.

The dependence of the location of our model's single ITCZ upon
the nature of the surface temperature profile is graphically illustrated
in figure 13. Recall from figure 12 that the Northern and Southern
hemisphere surface temperatures were last passing through maxima at
respectively the 130th and 156th week, one-half year apart. In figure
13 the temperature and precipitation profiles for these two periods
are shown; in each case the ITCZ is single and is located over the
surface temperature maximum in the warmer hemisphere. These two cases
are practically mirror-images of each other. One may easily imagine
how the quasi-symmetric rainfall profiles of figure 11 have been
generated by the single ITCZ alternating between hemispheres according
to which is warmer.

Whenever the hemispheric temperature asymmetry reverses, as at
the 140th week as indicated by figure 12, the model ITCZ shifts from
one hemisphere to the other with only a minor lag. Figure 14 illustrates
this process with four successive precipitation profiles. At the 138th
week the northern hemisphere is still definitely the warmer; its single
ITCZ at latitude 6N is well marked. There is some indication of a very
weak convergence zone at latitude 10S. Three weeks later the southern
hemisphere has become just a little warmer than the northern; at this
time the ITCZ has taken on a transitory double structure with the old
northern convergence zone approaching the equator and weakening over
the relatively cold water while a new, southern convergence zone is
developing at latitude 8S. By the 142nd week, the ITCZ is again sin-
gle, though still in a somewhat depressed state, and has clearly moved
across the equator into the warmer southern hemisphere. Two weeks
later, equatorial rainfall has ended and a single, re-invigorated
ITCZ is well established at latitude 8S.

The reduction in ITCZ precipitation during the period of tran-
sition between hemispheres is significant; the total rainfall rate,
proportional to the scaled area beneath the precipitation curves of
our figures, passes through a minimum at the 141st week which is fully
26 percent less than the mean rate of the 130th and 156th weeks; see
the data of figure 13. Recall that during these two weeks the hemispheric
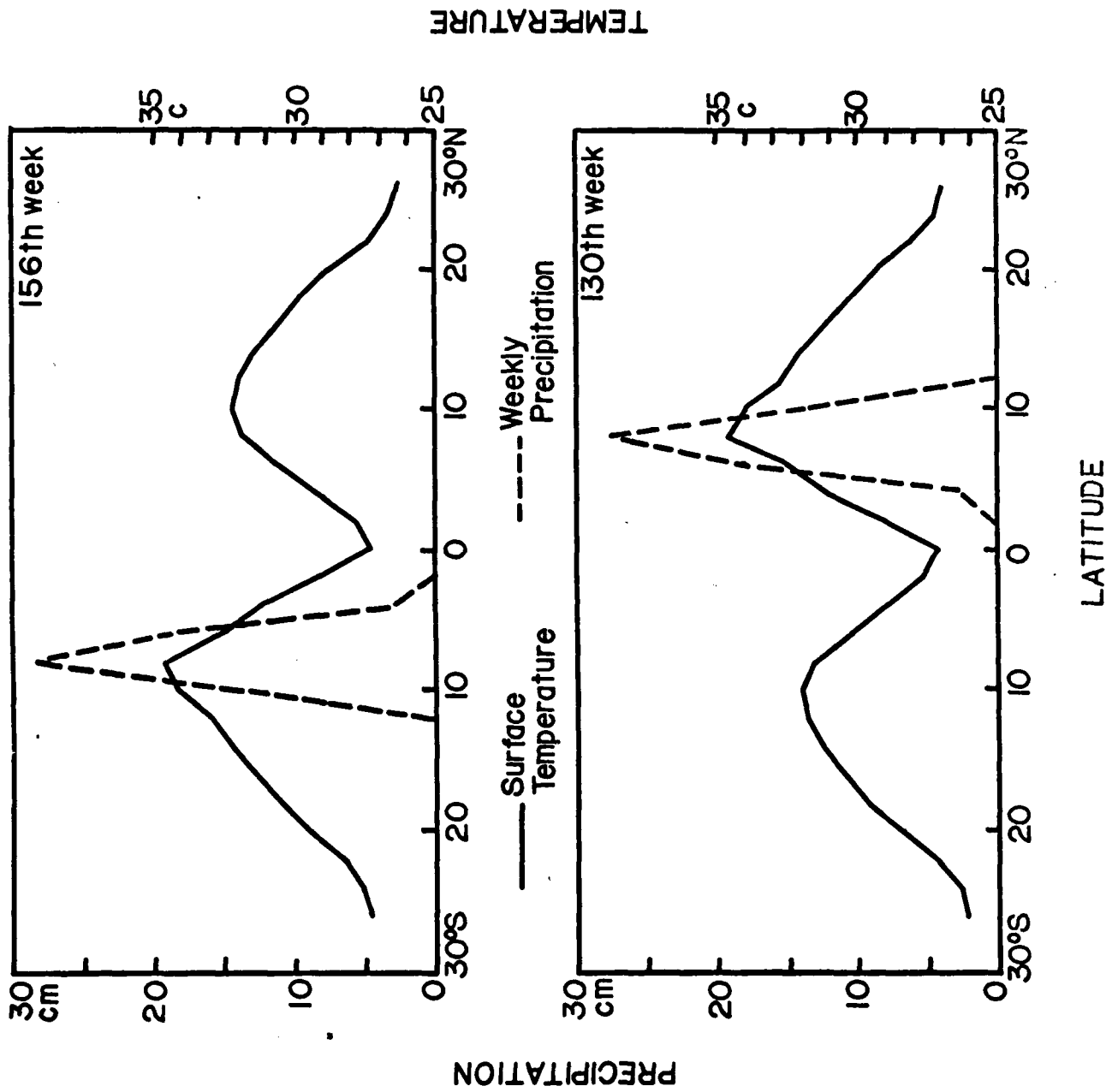thermal asymmetry was most pronounced and the ITCZ well developed. One

Fig. 13: Surface temperature and precipitation profiles, two cases
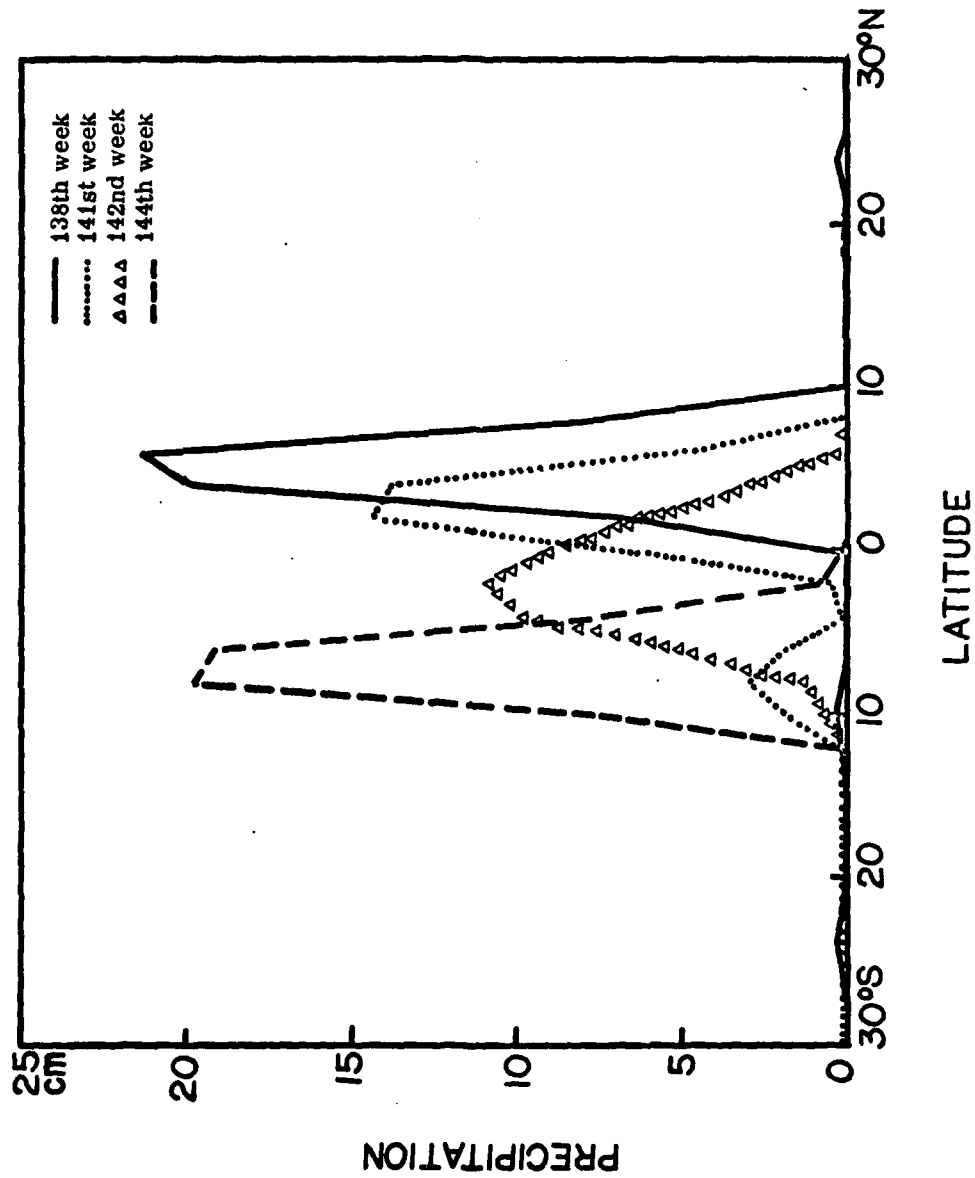one-half year apart.

Fig. 14: Precipitation profiles illustrating ITCZ transition between hemispheres.

physical reason for this temporary reduction is clear: during its transition across the equator, the ITCZ passes across the cooler equatorial water and is exposed to a reduced moisture source.

One would expect that whenever the ITCZ is precipitating less, the total moisture stored in the tropical atmosphere might be increased on account of the reduced condensation sink. To a relatively small extent this situation does happen in our model: at 141 weeks, when the ITCZ is weakest, the total moisture integrated over the whole model cross section passes through a maximum which is five percent greater than the average of the minima achieved at 126 and 152 weeks. Since this maximum occurs six weeks after a solstice, at mid-winter in one hemisphere and mid-summer in the other, the increase in stored moisture might supply extra available potential energy for extratropical storm development in the higher latitudes of the winter hemisphere and for tropical storm development in the subtropical latitudes of the summer hemisphere.

Probably the most disappointing aspect of the three-year experiments discussed above is the excessive warming of the sea surface and the resulting overheating of the atmosphere. Several shorter-term computations with the simplified interacting model have been carried out in an attempt to remedy this problem. Since the oceanic heat balance in its upper layer is composed primarily of incoming solar radiation and outgoing latent and sensible heat loss, it was decided to modify the adjustable parts of the model involved with these processes.

The solar heating in our model is very sensitive to the computed cloudiness, a function of the vertically-averaged relative humidity which in turn is partially dependent on the net radiative cooling. As the arbitrary specification of the vertical radiative cooling profile used in the three-year experiments was not particularly satisfying, it was decided that the modelling of this persistent effect should play the role of a negative feedback which ought to help stabilize the model thermally. It seemed reasonable to assume that, if $H_e(t)$ represents the total integrated enthalpy over the entire atmospheric cross-section of the model at time t, according to

$$H_e(t) = \int_{x_{-30}}^{x_{30}} \int_0^H \rho c_p T(t) dz dx \qquad (5.2)$$

then $H_e(t)$ should be set equal to $H_e(o)$ at all times since the cross-section is equally divided between hemispheres and one would expect its heat content very nearly to be conserved. If the radiational effect is given as a function of height by

$$\left(\frac{\partial T}{\partial t}\right)_R = \dot{T}_{Ro} f(z) \qquad (5.3)$$

then the integral in equation (5.2) may be conserved by letting

$$\dot{T}_{Ro} = \frac{H_e(o) - H_e(t)}{\Delta t \int_{x_{-30}}^{x_{30}} \int_o^H \rho c_p f(z) dz dx} \qquad (5.4)$$

The vertical shape function f(z) has been specified as [0.0, 0.5, 0.8, 1.0, 0.0], from the surface upward through the air model's vertical grid levels to the tropical tropopause; this profile is in agreement with the nature of the net radiative cooling as a function of height given for latitude 15 by Smagorinsky et al. (1965), p. 746. Equations (5.2) through (5.4) have been used in all our more recent model calculations, with the maximum cooling $T_{Ro}$ being calculated at ca.-1.0 C per day, a reasonable amount.

Modification of the surface evaporative and sensible heat fluxes may clearly be achieved by changing the surface drag coefficient $C_D$; see equation (3.8). These fluxes should be augmented, by increasing $C_D$, if surface cooling is the objective; such an increase may also require a larger vertical turbulent diffusivity $K_z$ in order to avoid trapping moisture in the surface boundary layer. The surface temperature profiles of figure 15 illustrate how sensitive this variable is to the adjustable coefficients of the vertical exchange processes. Three short-term experiments were made for 26 weeks, a half year, of physical time each to produce these profiles. Although the case with $C_D = 1.5\times10^{-3}$ and $K_z = 10^5 cm^2/sec$ may seem the coolest and the most realistic, these relatively low temperatures were partly influenced by excessive moistening of the middle atmosphere, and the resultant prediction of increased cloudiness and reduced surface solar insolation, on account of the large vertical diffusivity. This case also exhibited surface air temperatures higher than those of the sea surface; sensible heat was being diffused downward too vigorously. More satisfactory is the case with the same drag coefficient as above but with $K_z = 3\times10^4 cm^2/sec$; in this instance the only problem was with moisture saturation at the 1.057 km level.

The surface current components and mixed layer depth predicted by the oceanic portion of our long-term computations have not been illustrated in this section; their profiles are qualitatively similar to those obtained in the short-term interaction experiment discussed in section 2. Insidious deepening of the mixed layer continued to be present in the three-year experiments; in an effort to control this problem as well as to have more realistic sea temperatures at the model's edges, the lateral boundary conditions in the sea have been changed to specification, rather than prediction, of the current components, temperature and mixed layer depth at latitudes 30S and N. Fixing this depth at these points should allow the lateral diffusion term in equation (4.4) to operate more effectively in preventing excessive deepening; recent experiments are encouraging in this respect.
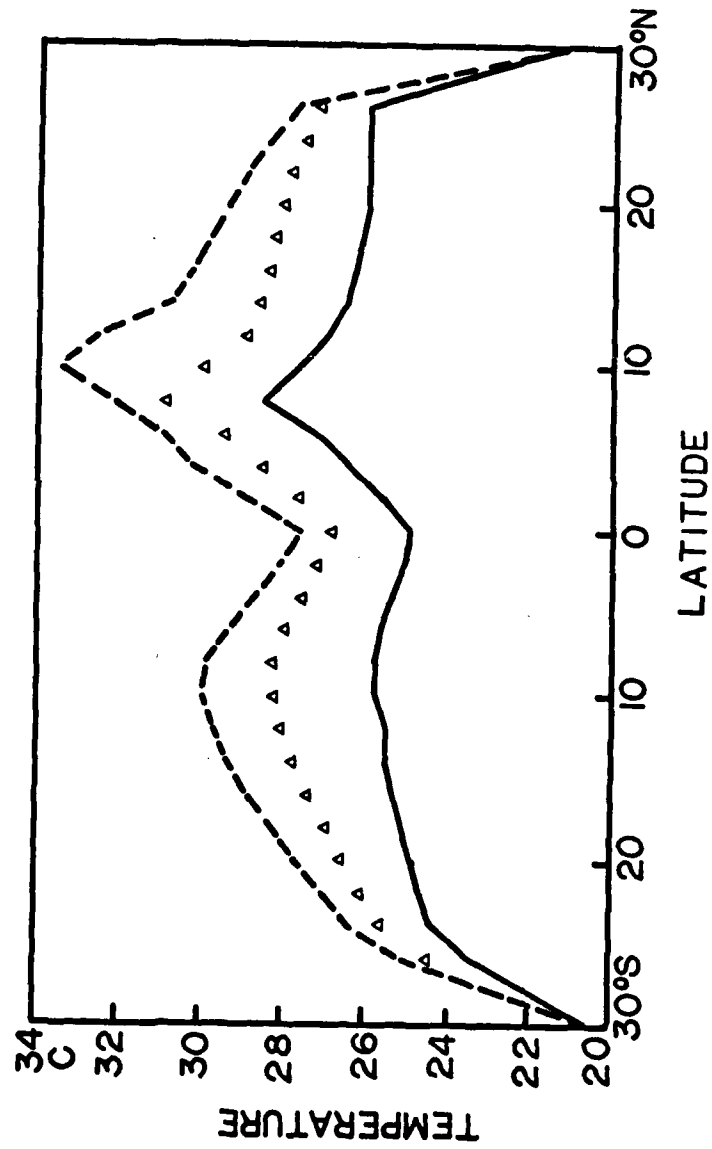
Fig. 15: Surface temperature profiles illustrating the importance of vertical exchange coefficients

## 6. Comparison of Results with Satellite and Conventional Observations

For the sake of brevity, no satellite cloud pictures will be pre-
sented here; instead, references will be given to some of the original
publications containing relevant photographic or interpretive material.

A word of caution is in order when comparing results from these
highly experimental fluid models with observations of the real atmosphere.
Since any model is bound to be less complex than reality, its conclu-
sions will always appear to be more straightforward than those drawn
from careful and comprehensive direct observations. Probably the best
compromise is to consider only those more gross observed features that
have obvious counterparts, whether accurately or crudely reproduced, in
the model.

It may fairly be assumed that theoretically computed precipitation
maxima should be ideally associated with observed total cloudiness
maxima, but not vice versa on account of non- or low- precipitating
stratiform clouds. Since our original, symmetrically-forced two-fluid
model experiment suggests that the equilibrium position of the oceanic
ITCZ rainfall peak is a few degrees of latitude away from the equator,
it is encouraging to note that Sadler (1969), using carefully analyzed
satellite data for 1965 and 1966, finds that the latitude of maximum
cloudiness in the tropics, averaged over all longitudes and taking an
average of winter and summer, is five degrees North; see his figure 4.
Sadler does not present a sea surface temperature analysis for the same
period as that of his observations; thus, no direct substantiation of
our theoretical findings with respect to the surface temperature pattern
is to be had from his analysis. One may only assume that long-term
climatological temperature maps such as those by Defant (1961) are
characteristic of most shorter periods.

Kornfield and Hasler (1969) present data comparable to Sadler's,
but for the year 1967 and in the form of computer-produced, time-
averaged pictures rather than processed diagrams. The oceanic ITCZ
in these photos clearly stays several degrees of latitude away from
the equator all year in the Pacific and most of the year, except for
the late Northern winter and early spring, in the Atlantic. In the
Indian Ocean strong monsoonal influences complicate the situation; but
it is suggested from both these and Sadler's data that here the equator
is more hospitable to occasional ITCZ formation than over other seas.
Fortunately, Defant's maps do indicate that equatorial cooling is far
less pronounced over the Indian Ocean all year and over the Atlantic
during the Northern winter than it usually is over the eastern and
central Pacific. An off-equator ITCZ is certainly observed over the
western Pacific, where the equatorial surface does not show nearly as
pronounced a temperature drop in meridional profile as it does farther
east; but this feature may be strongly influenced by zonal advection of
heat and moisture, from the east, that our two-dimensional model does
not duplicate in its meridional plane.

An interesting note by Hubert et al. (1969), using a year of satellite data partially overlapping those of Kornfield and Hasler, concludes that a single pronounced ITCZ cloudiness maximum with respect to latitude is much more common than a pronounced double maximum; i.e. that the actual ITCZ is usually hemispherically very asymmetric when off the equator. This observation applies at sea as well as over land. It is tempting to establish some connection between it and our original experimental results that a double ITCZ can have an unstable character in that one of its branches can dominate the other as in section 2 case II, while a single ITCZ appears to be comparatively stable, on or off the equator, as in section 2 case I and in the short-term interaction computation of that section. Note also that, except for a period of one week during the cross-equatorial shifting process, the ITCZ in the extended integrations of section 5 remained single. For the moment, all that may be said is that these observations do not conflict with our idea that the single ITCZ is the more stable configuration.

There have been some problems in comparing the detailed behavior of the ITCZ precipitation in our long-term experiments with satellite observations of the seasonal variation of ITCZ cloudiness in the real atmosphere. Sadler's (1969) zonally-averaged cloud data indicate that during the northern hemisphere summer a pronounced single cloudiness maximum is located at latitude 6N with no sign of any secondary maximum in the tropical southern hemisphere; this situation happens to be in good qualitative agreement with the prevailing ITCZ structure in the model. However, while during the southern hemisphere summer an expected cloudiness maximum does appear at latitude 8S, the maximum in the northern hemisphere persists - slightly closer to the equator. This winter-hemisphere maximum is less distinct than in the summer but still, in combination with the southern hemisphere feature, suggests a smeared double ITCZ of a type never present in the computations. Some conventional observations of the mean meridional circulation, to be discussed later, indicate that the winter tropical cloudiness of the northern hemisphere is probably associated on the zonal average with less upward air motion, and, therefore, with less rainfall, than is its southern summer companion.

Another interesting paper by Sadler (1970) uses satellite photography to study the transitional period when ITCZ cloudiness is increasing in one hemisphere and decreasing in the other. In this study, the observed changes in monthly mean cloudiness from one month to the next during this period are greatest at the off-equatorial latitudes where the ITCZ has been or will become well-formed in an approximately steady state. Inter-monthly mean cloudiness changes at the equator seem to be relatively minor. Sadler reasons from these observations that the ITCZ declines in one hemisphere while re-forming in the other without any cross-equatorial migration. Our model, on the other hand, does indicate such a migration, occurring over a period of about one month; see figure 14. The apparent discrepancy between these results may be resolved by noting that our experimental ITCZ weakens markedly while it is crossing the equator so that the magnitudes of rainfall rate, or cloudiness, changes at the equator are less than at

sub-equatorial latitudes. Also note that during inter-hemispheric migration, changes in ITCZ properties would be monotonic sufficiently far from the equator while at and near the equator these properties would pass through extrema, making their net changes relatively small over a sufficient lapse of time. We suspect that Sadler's averaging period may be too long to observe this kind of migration. With the aid of daily satellite pictures, Johnson (1969) observed frequent ITCZ movement across the equator in the Indian Ocean region.

It is much easier to compare the results of our long-term model computations with conventionally-derived observations of the mean meridional circulation of the tropics, e.g. Kidson et al. (1969) and Oort and Rasmusson (1970), than with any satellite cloud data. Kidson's tables and diagrams clearly show that the upward branch of the direct tropical Hadley cell is centered at about latitude 10N during the northern hemisphere summer and at about latitude 5S during the southern summer; at these latitudes during winter the mean vertical motion is very small - near a Hadley cell center, in fact. Kidson does not present observations for the transition seasons, but the data of Oort and Rasmusson show a very smooth migration of the tropical mean updraft across the equator during these periods. One notable difference between our experiments and the observed seasonal Hadley circulation is that in the former the width of the precipitation zone in each hemisphere is only about ten degrees of latitude while in the latter the updraft width is almost twice as great. This relative broadening is surely a result of the process of zonal averaging in the presence of the variation of land-sea distribution with longitude. In any event, our model does seem to approximate the seasonal behavior of the real tropical Hadley circulation fairly well with respect to location and structure. One would expect good results in this respect, compared to less good results when dealing with the relatively three-dimensional actual ITCZ, on account of our two-dimensional dynamics.

It is clear that the seasonal migration of this model's ITCZ is very closely related to the seasonal progress of its surface temperature; the same type of association is surely present in the real atmosphere. However, since the model's surface is purely oceanic while the earth's is partly continental, the lag characteristics, with respect to the solar heating, of this temperature and of the ITCZ will be different in the two cases. Since the real ITCZ rainfall is greatest over the Eastern Hemisphere continental and island region (Dickinson, 1970), the lag behind the equinoxes of the migration of the mean tropical rain belt across the meteorological equator is probably no more than eight weeks, as confirmed by the vertical motion data of Oort and Rasmusson (op.cit.). Over the real oceans the lag of the local ITCZ is somewhat greater. Assuming that the oceanic ITCZ crosses the meteorological equator at times halfway between the well-known northern and southern hemispheric tropical storm activity peaks in September and March respectively, one finds that here this lag is about one season, or 13 weeks. In our model, however, the tropical rainbelt is computed to cross the equator, which in this case is meteorological as well as geographic, fully 20 weeks after each equinox; see figures 12 and 14.

It should be borne in mind that atmospheric circulations over the real oceans are not at all independent of those over the continents; important telegraphic three-dimensional effects are bound to exist both thermally and dynamically; see Krueger and Gray (1969). Thus, even the oceanic ITCZ lag on Earth should be expected to be less than that on a completely oceanic globe on account of the relatively small surface-layer heat capacity on the continents. The 20-week lag seems to be physically realistic for our kind of model surface; it may be considered as the sum of seven weeks' lag between the equinox and the maximum ocean temperature plus the mandatory one season's lag between the maximum and median ocean temperatures. Since the maximum model surface temperatures occur between latitudes 5 and 10 degrees in space, they lag the overhead sun of late summer by about two months in time.

7. Summary

Several experiments with a forced, relatively sophisticated primitive equation model of the tropical atmospheric circulation, in a meridional plane, indicate clearly that the location of the oceanic intertropical convergence zone is influenced by the north-south profile of sea surface temperature. A definite maximum in surface temperature, on or off the equator, encourages atmospheric convergence, upward motion and active precipitation overhead or nearby. In the case of a relatively flat profile the major convergence zone forms over the equator, just as if there had been a temperature maximum there; in this model an equatorial temperature depression seems necessary to keep a stable ITCZ away. Here is good motivation to develop an interacting two-fluid model, including the upper ocean, in order to predict the surface temperature profile and its effects on tropical convection. Results from an 88-day integration of such a model, with an initially flat profile, show the progressive development of a cold equator on account of upwelling and vertical mixing of cold water in the sea. A single ITCZ establishes itself at first over the equator but then migrates poleward as the equator cools; the convergence zone remains single despite the eventual double surface temperature maximum. This marked hemispheric asymmetry appears to be of the same type noticed very often in satellite cloud pictures of the oceanic ITCZ.

Numerical integration of a two-fluid model over a period of several years seemed desirable in order to investigate the degree of stability of the single off-equatorial ITCZ under the influence of seasonally variable solar heating of the sea. The atmospheric part of the original interacting model was simplified to such an extent that a three-year integration could be accomplished in about 4-1/2 hours of CDC 6600 computer time.

As before, a cold equatorial surface developed while a single ITCZ formed and soon found a stable location, away from the equator, over the surface temperature maximum of the warmer hemisphere. The model ITCZ, in a temporarily weakened state, migrated quickly between hemispheres, with a lag of less than two weeks, whenever the progress of the seasons caused the hemispheric surface temperature asymmetry to reverse - every half year. This behavior is qualitatively in accord with that of

the updraft branch of the mean tropical Hadley circulation in the real atmosphere. The lag of the computed inter-hemispheric migration behind the solar equinox was 20 weeks, much longer than that of the observed mean tropical rainbelt on account of the lack of continents in our model. However, the lag of the maximum sub-equatorial sea surface temperature behind the overhead sun of late summer was computed at two months, a reasonable value for an ocean free of continental influences. The long-term experiments reinforced earlier results that a single ITCZ is the preferred mode in our kind of model; this mode appears to be more common than any other in the real atmosphere as well.

## 8. Acknowledgments

REFERENCES

Bates, J. R.: "Dynamics of disturbances on the intertropical convergence zone". Quarterly Journal of the Royal Meteorological Society, Vol. 96, 1970, pp. 677-701.

Budyko, M. I.: "The heat balance of the earth's surface". Translated by N. A. Stepanova, U. S. Dep't of Commerce, 1958, 259 pp. Original version published at Leningrad, 1956, 255 pp.

Defant, A.: Physical Oceanography, Vol. 1, Pergamon Press, London, 1961 729 pp.

Dickinson, R. E.: "Analytic Models for zonal winds in the tropics II. Variation of the tropospheric mean structure with season and differences between hemispheres". NCAR manuscript 70-76, Boulder Colo., 1970, 34 pp.

Estoque, M. A. and C. M. Bhumralkar: "Flow over a localized heat source". Monthly Weather Review, Vol. 97, 1969, pp. 850-859.

Hellerman, S.: "An updated estimate of the wind stress on the world ocean". Monthly Weather Review, Vol. 95, 1967, pp. 607-626.

Hubert, L. F. et al.: "The double intertropical convergence zone - fact or fiction?" Journal of the Atmospheric Sciences, Vol. 26, 1969, pp. 771-773.

Johnson, D. H.: "The role of the tropics in the global circulation". In The Global Circulation of the Atmosphere, Royal Meteorological Society, London, 1969, pp. 113-136.

Jordan, C. L.: "Mean soundings for the West Indies area". Journal of Meteorology, Vol. 15, 1958, pp. 91-97.

Kidson, J. W. et al: "Observational studies of the general circulation of the tropics: long-term mean values". Quarterly Journal of the Royal Meteorological Society, Vol. 95, 1969, pp. 258-287.

Kornfield, J. and A. F. Hasler: "A photographic summary of the Earth's cloud cover for the year 1967". Journal of Applied Meteorology, Vol. 8, 1969, pp. 687-700.

Kraus, E. B. and C. Rooth: "Temperature and steady state vertical heat flux in the ocean surface layers". Tellus, Vol.13, 1961, pp. 231-238.

Kraus, E. B. and J. S. Turner: "A one-dimensional model of the seasonal thermocline, Part II: The general theory and its consequences". Tellus, Vol. 19, 1967, pp. 98-106.

Krueger, A. F. and T. I. Gray, Jr.: "Long-term variations in equatorial circulation and rainfall". Monthly Weather Review, Vol. 97, 1969, pp. 700-711.

References (continued)


Manabe, S. and K. Bryan:  "Climate calculations with a combined ocean-
     atmosphere model".  Journal of the Atmospheric Sciences, Vol. 26,
     1969, pp. 786-789.

Murgatroyd, R. J.:  "Estimations from geostrophic trajectories of
     horizontal diffusivity in the mid-latitude troposphere and lower
     stratosphere".  Quarterly Journal of the Royal Meteorological
     Society, Vol. 95, 1969, pp. 40-62.

Oort, A. H. and E. M. Rasmusson:  "On the annual variation of the monthly
     mean meridional circulation".  Monthly Weather Review, Vol. 98,
     1970, pp. 423-442.

Peixoto, J. P.:  "Hemispheric temperature conditions during the year
     1950".  Planetary Circulations Project, scientific report no. 4, De-
     partment of Meteorology, Massachusetts Institute of Technology, 1960.

Peixoto, J. P. and A. R. Crisi:  "Hemispheric humidity conditions during
     the IGY".  Planetary Circulations Project, scientific report no. 6,
     Department of Meteorology, Massachusetts Institute of Technology, 1965.

Pike, A. C.:  "A numerical study of tropical atmospheric circulations".
     Air Force Cambridge Research Laboratories Scientific Report,
     document no. AFCRL-68-0593, 1968, 129 pp.  Available from
     Clearinghouse, U.S. Dept. of Commerce.

Pike, A. C.:  "The inter-tropical convergence zone studied with an
     interacting atmosphere and ocean model".  Air Force Cambridge
     Research Laboratories Scientific Report, document no. AFCRL-70-0069,
     1970, 29 pp.  Available from Clearinghouse, U.S. Dept. of Commerce.

Richtmyer, R. D. and K. W. Morton:  Difference Methods for Initial-Value
     Problems, second edition.  Interscience Publishers, New York, 1967,
     405 pp.

Sadler, J. C.:  Average cloudiness in the tropics from satellite obser-
     vations.  East-West Center Press, Honolulu, 1969, 23 pp.

Sadler, J. C.:  "Does the convergence zone migrate between hemispheres?"
     In Proceedings Symposium Tropical Meteorology, American Meteorological
     Society, Boston, 1970.

Smagorinsky, J. et al.:  "Numerical results from a nine-level general
     circulation model of the atmosphere".  Monthly Weather Review,
     Vol. 93, 1965, pp. 727-798.

Stommel, H.:  The Gulf Stream.  University of California Press, Berkeley,
     1966, 248 pp.

Turner, J. S.:  "A note on wind mixing at the seasonal thermocline".
     Deep-Sea Research, Supplement to Vol. 16, 1969, pp. 297-300.

References (continued)

Weather Bureau, U. S. Department of Commerce:  World Weather Records,
     1941-1950.  U. S. Government Printing Office, Washington, 1959,
     1361 pp.

Wyrtki, K.:  The thermal structure of the eastern Pacific ocean.
     Deutsches Hydrographisches Institut, Hamburg, 1964, 84 pp.

Yamasaki, M.:  "A tropical cyclone model with parameterized vertical
     partition of released latent heat".  Journal of the Meteorological
     Society of Japan, Vol. 46, 1968, pp. 202-214.

## DOCUMENT CONTROL DATA - R & D

*(Security classification of title, body of abstract and indexing annotation must be entered when the overall report is classified)*

| 1. ORIGINATING ACTIVITY (Corporate author) | 2a. REPORT SECURITY CLASSIFICATION |
|---|---|
| University of Miami, School of Marine and Atmospheric Science, Div. of Atmos. Science Coral Gables, Florida 33124 | Unclassified |
| | 2b. GROUP |

**3. REPORT TITLE**

SEASONAL VARIATIONS OF THE INTER-TROPICAL CONVERGENCE ZONE STUDIED WITH AN INTERACTING ATMOSPHERE AND OCEAN MODEL

**4. DESCRIPTIVE NOTES (Type of report and inclusive dates)**

Scientific    Final, November 1967 - January 1971    Approved 18 February 1971

**5. AUTHOR(S) (First name, middle initial, last name)**

Arthur C. Pike

| 6. REPORT DATE | 7a. TOTAL NO. OF PAGES | 7b. NO. OF REFS |
|---|---|---|
| January 1971 | 48 | 30 |

| 8a. CONTRACT OR GRANT NO. | 9a. ORIGINATOR'S REPORT NUMBER(S) |
|---|---|
| F19628-68-C-0144 | |
| b. PROJECT, TASK, AND WORK UNIT NO. 6698-02-01 | --- |
| c. DOD ELEMENT 62101F | 9b. OTHER REPORT NO(S) (Any other numbers that may be assigned this report) |
| d. DOD SUBELEMENT 681000 | AFCRL-71-0067 |

**10. DISTRIBUTION STATEMENT**

1 - This document has been approved for public release and sale; its distribution is unlimited.

| 11. SUPPLEMENTARY NOTES | 12. SPONSORING MILITARY ACTIVITY |
|---|---|
| TECH, OTHER | Air Force Cambridge Research Laboratories (LY) L. G. Hanscom Field Bedford, Massachusetts 01730 |

**13. ABSTRACT**

A simple, four-level primitive-equation model of a zonally-symmetric tropical atmosphere has been combined with a two-layer model of the upper tropical ocean in order to predict three years of inter-tropical convergence zone (ITCZ) behavior under the influence of seasonally-variable solar heating of the sea. A cold equatorial surface develops on account of oceanic upwelling and vertical mixing; a single ITCZ establishes itself, off the equator, over the surface temperature maximum in the warmer hemisphere. This convergence zone migrates quickly between hemispheres, with only a minor lag, when the progress of the seasons causes the hemispheric surface temperature asymmetry to reverse every half year. Such behavior is qualitatively in accord with that of the updraft branch of the mean tropical Hadley circulation in the real atmosphere. The lag of maximum sub-equatorial sea surface temperature behind the overhead sun of late summer is computed to be about nine weeks, a reasonable value.

DD FORM 1473
1 NOV 65

| KEY WORDS | LINK A | | LINK B | | LINK C | |
|---|---|---|---|---|---|---|
| | ROLE | WT | ROLE | WT | ROLE | WT |
| Numerical model | | | | | | |
| Seasonal variations | | | | | | |
| Tropical atmosphere | | | | | | |
| Inter-tropical convergence zone | | | | | | |
| Precipitation | | | | | | |
| Tropical ocean | | | | | | |
| Air-sea interaction | | | | | | |
| Sea surface temperature | | | | | | |